



RESEARCH ARTICLE

10.1002/2015JC011599

Carbon exchange between a shelf sea and the ocean: The Hebrides Shelf, west of Scotland

Stuart C. Painter¹, Susan E. Hartman¹, Caroline Kivimäe¹, Lesley A. Salt², Nicola M. Clargo³, Yann Bozec², Chris J. Daniels¹, Sam C. Jones^{4,5}, Victoria S. Hemsley^{1,6}, Lucie R. Munns^{1,6}, and Stephanie R. Allen^{1,6}

¹National Oceanography Centre, European Way, Southampton, UK, ²Sorbonnes Universités, UPMC Univ Paris 06, CNRS, UMR 7144 Adaptation et Diversité en Milieu Marin, Station Biologique de Roscoff, Place Georges Teissier, Roscoff, France, ³Royal Netherlands Institute for Sea Research, Texel, Netherlands, ⁴Scottish Association for Marine Science, Oban, UK, ⁵Department of Physics, University of Aberdeen, Aberdeen, UK, ⁶University of Southampton, National Oceanography Centre, Ocean and Earth Science, European Way, Southampton, UK

Key Points:

- Cross-shelf transports and carbon fluxes are reported for the Hebrides Shelf
- The mean Ekman drain downslope transport was $1.81 \text{ m}^2 \text{ s}^{-1}$, but important 4-fold spatial variability was identified
- The Hebrides Shelf may export 5 times more POC per unit area via the Ekman drain than the global mean

Correspondence to:

S. C. Painter,
stuart.painter@noc.ac.uk

Citation:

Painter, S. C., et al. (2016), Carbon exchange between a shelf sea and the ocean: The Hebrides Shelf, west of Scotland, *J. Geophys. Res. Oceans*, 121, 4522–4544, doi:10.1002/2015JC011599.

Received 22 DEC 2015

Accepted 21 MAY 2016

Accepted article online 26 MAY 2016

Published online 2 JUL 2016

Corrected 28 JUL 2016

This article was corrected on 28 JUL 2016. See the end of the full text for details.

Abstract Global mass balance calculations indicate the majority of particulate organic carbon (POC) exported from shelf seas is transferred via downslope exchange processes. Here we demonstrate the downslope flux of POC from the Hebrides Shelf is approximately 3- to 5-fold larger per unit length/area than the global mean. To reach this conclusion, we quantified the offshore transport of particulate and dissolved carbon fractions via the “Ekman Drain,” a strong downwelling feature of the NW European Shelf circulation, and subsequently compared these fluxes to simultaneous regional air-sea CO_2 fluxes and onshore wind-driven Ekman fluxes to constrain the carbon dynamics of this shelf. Along the shelf break, we estimate a mean offshore total carbon (dissolved + particulate) flux of $4.2 \text{ tonnes C m}^{-1} \text{ d}^{-1}$ compared to an onshelf flux of $4.5 \text{ tonnes C m}^{-1} \text{ d}^{-1}$. Organic carbon represented 3.3% of the onshelf carbon flux but 6.4% of the offshore flux indicating net organic carbon export. Dissolved organic carbon represented 95% and POC 5% of the exported organic carbon pool. When scaled along the shelf break the total offshore POC flux ($0.007 \text{ Tg C d}^{-1}$) was found to be 3 times larger than the regional air-sea CO_2 ingassing flux ($0.0021 \text{ Tg C d}^{-1}$), an order of magnitude larger than the particulate inorganic carbon flux ($0.0003 \text{ Tg C d}^{-1}$) but far smaller than the DIC (2.03 Tg C d^{-1}) or DOC (0.13 Tg C d^{-1}) fluxes. Significant spatial heterogeneity in the Ekman drain transport confirms that offshore carbon fluxes via this mechanism are also spatially heterogeneous.

1. Introduction

The temperate coastal ocean is an important sink for atmospheric CO_2 but changing environmental conditions are likely to alter the effectiveness of this sink in future [Bauer et al., 2013; Regnier et al., 2013]. Initial estimates extrapolated from the East China Sea suggested the global coastal ocean absorbed almost 1 Pg C yr^{-1} [Tsunogai et al., 1999]. Continued improvement in observational capability, data synthesis activities, and analytical methodologies, however, has resulted in a progressive decrease in the magnitude of this sink term (see summary in Chen et al. [2013]) with one recent estimate suggesting a global carbon sink in coastal seas of $\sim 0.2 \text{ Pg C yr}^{-1}$ [Laruelle et al., 2014]. Despite efforts to improve estimates of the global CO_2 sink in coastal seas there is still considerable uncertainty in the contribution of individual shelf seas to regional carbon budgets, a situation that precludes accurate prediction of future events [Borges, 2005].

The Northwest European Shelf is one of the best-studied continental shelf regions in the world with data coverage that is considered sufficient to allow calculation of seasonal air-sea CO_2 fluxes with high confidence [Thomas et al., 2004; Chen et al., 2013; Laruelle et al., 2014]. The Hebrides Shelf, to the west of Scotland, makes up the north-western extremity of the NW European Shelf and accounts for $\sim 7\%$ of the total area of the NW European Shelf. It is, however, a region of significant exchange of water with the open ocean with models and long-term observations suggesting typical onshore wind-driven exchanges and compensating downwelling offshore fluxes of $\sim 1 \text{ Sv}$ [Holt et al., 2009; Huthnance et al., 2009; Huthnance, 2010; Wake-*lin et al.*, 2012]. The strong downwelling circulation along the Hebrides Shelf edge, and more widely along the NW European Shelf edge, is considered a vital conduit for the export of carbon to the open ocean but it

© 2016. The Authors.

This is an open access article under the terms of the Creative Commons Attribution License, which permits use, distribution and reproduction in any medium, provided the original work is properly cited.

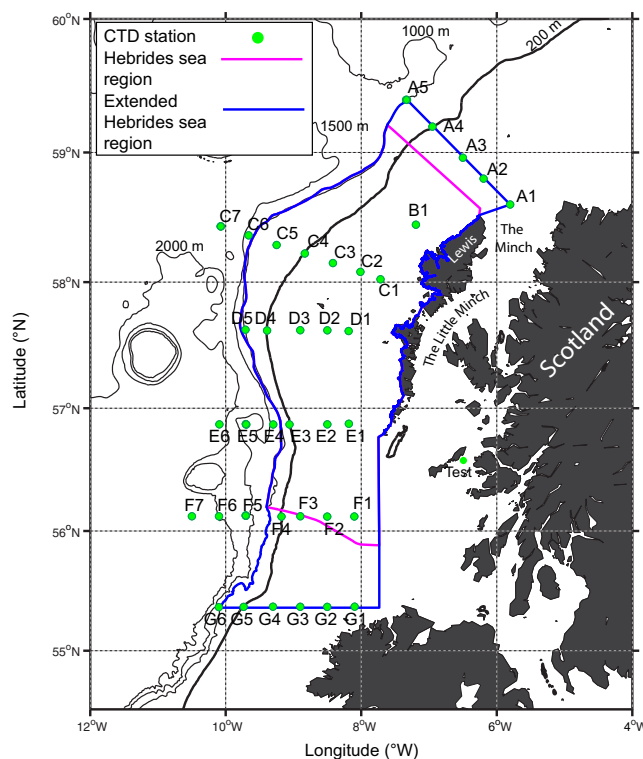


Figure 1. Map of the survey area denoting position of sampling stations.

remains poorly constrained observationally [Holt *et al.*, 2009; Huthnance *et al.*, 2009; Wakelin *et al.*, 2012; Simpson and McCandliss, 2013].

The downwelling circulation is induced by the European Slope Current, a warm and saline northerly flowing current located over the upper continental slope of the NW European shelf that is considered an important route for the transfer of heat and salt to the Arctic, and which in winter, likely runs continuously from the Bay of Biscay to the Norwegian Sea [Huthnance, 1986; Pingree, 1993; Xu *et al.*, 2015]. The Slope Current is typically centered above the 500 m bathymetric contour, generally below the seasonal thermocline, and closely follows the bathymetry northward [Booth and Ellett, 1983]. Measurements within the Slope Current indicate typical current velocities of $0.2\text{--}0.4\text{ m s}^{-1}$, and transports of $\sim 1.5\text{ Sv}$, though there is considerable variability with latitude and by season with increased current velocities and

transports northward and throughout autumn and winter [Dickson *et al.*, 1986; Huthnance 1986; Carter *et al.*, 1987; Xu *et al.*, 2015]. Over the inner shelf, and predominately inshore of the Hebridean Islands, runs the Scottish Coastal Current, another northward flowing current, with a mean velocity of $\sim 0.11\text{ m s}^{-1}$ and a volume transport of $\sim 0.1\text{ Sv}$ [McKay *et al.*, 1986; Inall *et al.*, 2009]. In addition to distinct currents, a residual northward flow exists over the wider Hebrides Shelf [McKay *et al.*, 1986; Xing and Davies, 1996]. Near-geostrophy within the Slope Current greatly restricts direct cross-shelf exchange with the open ocean and long-term observations indicate typical cross-shelf current velocities of $< 0.04\text{ m s}^{-1}$ [Booth and Ellett, 1983; Huthnance, 1986; Souza *et al.*, 2001; Simpson and McCandliss, 2013]. However, a strong cross-shelf downwelling circulation is induced under the Slope Current via frictional stresses within the bottom boundary layer overcoming geostrophic control. This process, known as the “Ekman Drain,” can result in significant offshore transport close to the seabed. Limited observational evidence suggests a particulate carbon flux of $30\text{ kmol C m}^{-1}\text{ yr}^{-1}$ ($0.36\text{ tonnes C m}^{-1}\text{ yr}^{-1}$) associated with the Ekman drain along the Hebrides Shelf [Simpson and McCandliss, 2013]. Model estimates, however, differ markedly with the modeled flux of $23\text{--}41\text{ kmol C m}^{-1}\text{ yr}^{-1}$ obtained by Proctor *et al.* [2003] being far smaller than the total organic carbon flux of $180\text{ kmol C m}^{-1}\text{ yr}^{-1}$ derived from the model results of Wakelin *et al.* [2012], indicating that additional observational constraints of the various carbon pools and fluxes are needed.

In this study, we simultaneously estimate the cross-shelf downwelling transport, the wind-driven surface Ekman transport, the associated fluxes of carbon and the air-sea CO_2 flux from new observations on the Hebrides Shelf to determine the significance of all terms to a regional carbon budget.

2. Methods

During October and November 2014, six cross-shelf transects were undertaken between 55.3°N and $\sim 59.2^\circ\text{N}$ (Figure 1). A total of 56 full-depth CTD casts were conducted at 37 stations with water samples collected from 5 to 24 depths at each station. Water column depths ranged from 75 to $\sim 2100\text{ m}$ and transect lengths varied from ~ 80 to $\sim 140\text{ km}$ with an average along-track station spacing of 24 km. Bad weather prevented the completion of transect B.

Marine Scotland designate seven “sea regions” around Scotland for statutory purposes which includes the Hebrides Sea Region, a formally designated area of 41,134 km² stretching westward from the west coast of the Hebrides Islands to the 1000 m bathymetric contour and from ~56°N to ~59°N [Baxter *et al.*, 2011]. This region is smaller than that sampled during the cruise (Figure 1) so to formulate regional fluxes utilizing all available data we extended the geographical limits of this sea region to the northern and southern extremities of our data (~55.3–59.2°N) while maintaining the 1000 m contour as the western boundary and the nominal inshore eastern boundary at 7.8°W (Figure 1). This new extended region covers ~54,747 km², and represents approximately 5% of the total area of the NW European Shelf (1112 × 10³ km²).

2.1. Nutrients

Concentrations of nitrate (NO₃ + NO₂; hereafter nitrate), phosphate (PO₄³⁻), and silicic acid [Si(OH)₄; hereafter silicate] were measured on discrete water samples collected via CTD/rosette sampling. Water samples were collected from all sampled depths direct from CTD Niskin bottles into 25 ml plastic vials and analyzed immediately or refrigerated at 4°C until analysis. All samples were analyzed on a Skalar Sanplus autoanalyser using common methodologies [e.g., Kirkwood, 1996; Hydes *et al.*, 2010].

2.2. Dissolved Inorganic Carbon and Total Alkalinity

Dissolved inorganic carbon (DIC) and total alkalinity (T_A) were sampled and measured according to best practice procedures [Dickson *et al.*, 2007]. 0.6 liter water samples were collected from the CTD Niskin bottles at all sampled depths and stations into borosilicate glass bottles with plastic caps using tygon tubing. Analysis commenced immediately after sampling in a temperature controlled laboratory using two VINDTA 3C instruments. A fresh bottle of certified reference material (CRM, Batch 140) was used to ensure accuracy for each station and all analyses were completed within 12 h of sampling. The analytical precision based on replicate CRM analysis was ±2.2 μmol kg⁻¹ for alkalinity and ±2.07 μmol kg⁻¹ for DIC.

2.3. Vessel Mounted Acoustic Doppler Current Profiler

RRS *Discovery* is fitted with 75 and 150 kHz RDI “Ocean Surveyor” Acoustic Doppler Current profilers (ADCP). We preferentially used the 75 kHz instrument due to its deeper acoustic penetration and during the cruise this was set to operate in “narrowband” mode and to average over 120 s intervals with 60 depth bins of 16 m thickness with data acquisition via VM-DAS. Preliminary data processing at sea corrected for instrument mis-alignment angle and vessel motion as described in best-practice guidelines [Firing and Hummon, 2010]. Technical problems with the operation of the instrument while at sea however resulted in intermittent 3- and 4-beam solutions, with the problem eventually traced to a faulty deck-unit, which was swapped midcruise resulting in consistent 4-beam solutions thereafter. Consequently usable data only exist for part of transect C and along transects D–G. Data from the 150 kHz instrument are used to provide current information along transect A.

Inspection of the data after the cruise identified several additional problems with data coverage and beam penetration into the water column so the entire data set was reprocessed using the Python based “CODAS processing” routines developed by the University of Hawaii (http://currents.soest.hawaii.edu/docs/adcp_doc/index.html). The reprocessing of the data resulted in the production of a data set with a 10 m vertical bin resolution and a 15 min averaging period (5 m vertical resolution for the 150 kHz data).

The VM-ADCP data were detided to remove barotropic tidal oscillations using Oregon State University's Ocean Topography Experiment/Poseidon Cross Over Global Inverse Solution [Egbert *et al.*, 1994; Egbert and Erofeeva, 2002] using a 1/30th degree resolution tidal model of the northwest European Shelf [Egbert *et al.*, 2010; model available at <http://volkov.oce.orst.edu/tides/>] and a Matlab-based toolbox to access and extract the tidal components (http://polaris.esr.org/ptm_index.html).

2.4. Hydrography

CTD salinity measurements were calibrated against water samples analyzed using a Guildline Autosol salinometer and IAPSO seawater standards (P-series). All hydrographic parameters are reported using the new Thermodynamic Equation of State (TEOS-10) terminology (i.e., Conservative Temperature (Θ;°C) and Absolute Salinity (S_A ; units g kg⁻¹) [IOC SCOR and IAPSO, 2010].

2.5. Dissolved Oxygen

Dissolved oxygen concentrations were measured in duplicate using the Winkler whole bottle technique [Langdon, 2010]. Up to 12 depths on each CTD cast were sampled. The accuracy of the measurements based on duplicate samples was estimated at $\pm 0.3 \mu\text{mol kg}^{-1}$. Discrete oxygen measurements were used to calibrate the Seabird-43 dissolved oxygen sensor attached to the CTD rosette frame according to Uchida *et al.* [2010].

2.6. Particulate Material

Several classes of particulate material were sampled for during the cruise. These included particulate organic carbon (POC) and particulate organic nitrogen (PON). Concentrations of both were measured on 1 L seawater samples filtered on to preashed ($>450^\circ\text{C}$ for >4 h) 25 mm glass fiber filters (Whatman GF/F). After filtration samples were twice rinsed with a weak 1% solution of HCL to remove inorganic carbon. Filters were oven dried at 40°C before being pelleted into tin capsules and analyzed for carbon and nitrogen content using a Costech ECS 4010 CHN elemental analyzer.

Particulate organic phosphate (POP) concentrations were measured using the method described by Raimbault *et al.* [1999]. Briefly, 1 L seawater samples were filtered onto precombusted, acid washed (10% HCL) GF/F filters, oven dried, and stored in sealed precombusted glass test tubes until analysis. In the laboratory, each filter was transferred to a pyrex screw top test tube (HDPE screwcap with Teflon liner) and a sodium tetraborate/potassium peroxodisulphate oxidizing reagent added. Each tube was tightly sealed and placed in an autoclave at 121°C for 30 min. Thereafter, the sample was centrifuged at 3000 rpm for 30 min before the phosphate content was measured by autoanalyser. Oxidation efficiency was assessed via parallel oxidation of an organic reference standard (NIST reference material 1573a, "Tomato Leaves"). Oxidation efficiency ranged from 79% to 85%. Consequently, sample POP content was increased by an amount based on the average oxidation efficiency for each batch of samples analyzed.

Biogenic silica (bSi) concentrations were measured using the method of Ragueneau and Treguer [1994]. Briefly, a 0.5 L sample was filtered onto a 25 mm diameter $0.8 \mu\text{m}$ polycarbonate filter, which was dried at 40°C and stored in 15 ml Falcon tubes until alkaline digestion and analysis for the Si content could be undertaken. In the laboratory, 5 ml of 0.2 M NaOH was added to each Falcon tube to digest the sample, which was baked at 85°C for at least 2 h. After returning to room temperature approximately 10 ml of 0.1 M HCL was added to neutralize the pH of the digested sample to pH 7–8. The solution was then analyzed by autoanalyser as described above for Si analysis. Note that results are reported both as the measured molar concentration of $\text{Si}(\text{OH})_4$ when describing typical bSi distributions or are converted to mass of opal assuming a molecular formula of $\text{SiO}_2 \cdot 0.4 \text{H}_2\text{O}$ when describing cross-shelf fluxes. Analytical blanks (fresh filters washed with $0.2 \mu\text{m}$ filtered seawater) were treated as above.

Particulate inorganic carbon (PIC) concentrations were typically measured on a surface sample only and on 0.5 L seawater samples filtered on to 25 mm $0.2 \mu\text{m}$ polycarbonate filters. Each filter was rinsed with a weak solution of analytical grade ammonium solution (pH ~ 9.7) to remove residual sea salt and placed in a 2 ml Eppendorf tube. Filters were oven dried at 40°C and stored until analysis. In the laboratory, all samples were weighed, extracted in 3% nitric acid and analyzed using Inductively Coupled Plasma Atomic Mass Spectrometry [Green *et al.*, 2003]. Sample carbon content (as PIC) was calculated assuming a 1:1 molar equivalency with the measured calcium content (present as CaCO_3) of the sample [Van Bleijswijk *et al.*, 1994].

2.7. Exchange Rate Calculations

2.7.1. Air-Sea Flux of CO_2

Estimates of the air-sea CO_2 flux were calculated using a common bulk methodology [e.g., Laruelle *et al.*, 2014]. At each station, the instantaneous flux of CO_2 was calculated as

$$\text{Flux } \text{CO}_2 = k \cdot K'_0 \cdot \Delta p\text{CO}_2 \quad (1)$$

where k is the gas transfer velocity (m s^{-1}), K'_0 is the CO_2 gas saturation constant calculated from Weiss [1974] using appropriate temperature (in K) and salinity measurements, and $\Delta p\text{CO}_2$ is the difference in partial pressure between seawater and the atmosphere.

The gas transfer velocity was calculated from

$$k = \Gamma C U^2 \left(\frac{Sc}{660} \right)^{-1/2} \quad (2)$$

where Γ is the transfer coefficient (0.26) of *Takahashi et al.* [2009], U is the wind speed 10 m above the sea surface, C is a correction factor suggested by *Jiang et al.* [2008], and Sc is the Schmidt number formulated according to *Wanninkhof* [1992]

$$Sc = 2073.1 - 125.62 \cdot SST + 3.6276 \cdot SST^2 - 0.043219 \cdot SST^3 \quad (3)$$

where SST is taken from the in situ measurements.

Due to the failure of the ship fitted meteorological instrument suite, we have taken wind speed estimates from the ECMWF global reanalysis product (ERA-Interim), which provides 6 hourly estimates of wind speed on a global 0.75×0.75 deg grid. Wind speeds were linearly interpolated from the ERA-Interim product to the time and position of the sampled stations. Use of this data product necessitated subsequent use of the correction factor (C) suggested by *Jiang et al.* [2008] to account for nonlinearity between wind speed and gas transfer relationships

$$C = \frac{\frac{1}{n} \sum_j U_j^2}{U_{\text{mean}}^2} \quad (4)$$

where U_j is the 6 hourly wind speed estimate and U_{mean} is the mean wind speed over the study period.

Atmospheric $p\text{CO}_2$ was calculated as

$$(p\text{CO}_2)_{\text{air}} = X\text{CO}_2 \cdot (P_{\text{baro}} - P_{\text{sw}}) \quad (5)$$

where $X\text{CO}_2$ is the mean CO_2 concentration for dry air for October and November 2014 (396.935 ppm) taken from the NOAA global CO_2 record (<http://www.esrl.noaa.gov/gmd/ccgg/trends/global.html>), P_{baro} is barometric pressure at the sea surface interpolated to the time and location of sampling and taken from NCEP-II reanalysis products [*Kanamitsu et al.*, 2002]; a global 6 hourly product on a 2.5×2.5 deg resolution grid, and P_{sw} is the water vapor pressure at the in situ temperature and salinity calculated according to *Weiss and Price* [1980].

We calculated estimates of $(p\text{CO}_2)_{\text{sw}}$ corrected to in situ sampling temperatures from the Excel based version of CO_2SYS described by *Pelletier et al.* [2007] (version 25b06), using the measured DIC and alkalinity as input and using recommended constants throughout [*Dickson et al.*, 2007; *Orr et al.*, 2015].

Finally, we calculated the difference in partial pressure between seawater and the atmosphere as

$$\Delta p\text{CO}_2 = (p\text{CO}_2)_{\text{sw}} - (p\text{CO}_2)_{\text{air}} \quad (6)$$

In addition to the daily flux estimates obtained for each station, we also calculated a large area daily integral of CO_2 flux based on the mean station flux and the extended Hebrides Sea Region defined above. This spatial area encompassed 78% of the available data with the remaining 22% of observations located over deep waters off shelf.

2.8. Shelf-Edge Exchange and the Flux of Biogenic Material

Cross-shelf exchange via the Ekman drain was estimated following the theoretical arguments presented by *Souza et al.* [2001] and *Simpson and McCandliss* [2013] which relate barotropic current velocities to downslope cross-shelf exchange via the equation

$$Tb = \frac{K_b \bar{V}^2}{f} \quad (7)$$

where Tb is the downslope transport in the bottom Ekman Layer (units $\text{m}^2 \text{s}^{-1}$), K_b is the bottom drag coefficient (0.0025, unitless), \bar{V} is the depth-averaged current (m s^{-1}), and f the Coriolis parameter. Where possible we calculated the maximum depth-averaged meridional current (V) for each transect corresponding to the core of the Slope Current from the detided VM-ADCP data. The exception being transect A where, due to the rotation of the current around the continental shelf bathymetry, we used the zonal current (U). This was then used as input to equation (7) to estimate the downslope transport for each transect (units of m^2)

s^{-1}). Shelf wide horizontal volume transports ($m^3 s^{-1}$) were subsequently calculated by multiplying the transport estimate from each transect by the length of the slope (516 km; determined as the distance along the 200 m bathymetric contour between the southernmost and northernmost transects). This resulted in six separate estimates of shelf wide volume transport.

To estimate the associated flux of biogenic material to the open ocean via the Ekman drain, we considered two different approaches. In the first simpler approach, particulate pool concentrations near the seabed at each shelf break station were identified. This provided particulate pool concentrations over a depth range of 187–224 m (in water depths of 195–237 m), comparable to the depth range that the Ekman drain is considered to operate over [Huthnance *et al.*, 2009; Wakelin *et al.*, 2012], but with limited information regarding lateral gradients. In the second approach, we calculated a mean concentration for each transect using the deepest samples for shelf and shelf break stations only. This included samples collected over a depth range of 60–224 m and while revealing important heterogeneity in particulate distributions near the seabed, with higher concentrations eastward onto the shelf, may bias upward the representative concentration entrained into the Ekman drain. Surprisingly, despite differences in particulate concentrations of up to $\pm 30\%$ between the two approaches on each transect (i.e., shelf break versus transect average concentrations could differ by up to $\pm 30\%$), only modest differences in the overall shelf wide mean particulate concentrations were found suggesting that mean regional fluxes from either method will give comparable results. For example, the mean POC concentration at shelf break stations was 89 mg m^{-3} compared to a mean of 86 mg m^{-3} for all shelf and shelf break stations. Nevertheless, due to the lateral variability in particulate concentration along each transect and the sensitivity in the calculation of material flux to that variability we have used the shelf break stations only in our calculations. Consequently, near seabed concentrations of POC, PON, POP, and bSi-opal at the shelf break were multiplied by the transport calculated for each transect to obtain the downslope fluxes of material associated with each transect. A similar approach was followed for dissolved constituents. Where stated, the total offshore export for the Hebrides Shelf is based on the overall mean flux (i.e., the mean of all transect fluxes) and typically reported in units of weight per meter of shelf edge per day (e.g., tonnes $C \text{ m}^{-1} \text{ d}^{-1}$). Exceptions to this occur when extrapolations of individual fluxes along the shelf break are undertaken to estimate the total offshore flux for the region studied (e.g. $Tg \text{ C d}^{-1}$). We have avoided, where possible, the extrapolation of daily fluxes to an annual basis due to an absence of seasonal information on the variability in the Slope Current and in particulate/dissolved concentrations.

Estimates of the surface wind-driven Ekman flux (T_E) were calculated for comparison to the Ekman drainage flux following Huthnance *et al.* [2009] using ERA-Interim wind speeds and directions; specifically

$$T_E = \rho_a C_D (W^2 \cos \theta + w'^2) / (\rho_w f) \quad (8)$$

where $\rho_a = 1.25$ and $\rho_w = 1027$ are the densities (kg m^{-3}) of air and seawater, $C_D = 0.0012$ is the drag coefficient, W is the monthly mean wind speed calculated for the period 15 October to 15 November 2014, θ is the angle of the wind relative to the orientation of the shelf, w' is the standard deviation of the wind speed in the along slope direction, and f is the coriolis parameter. Onshore carbon fluxes were calculated in a similar manner to the Ekman drain fluxes except for the use of mean mixed layer concentrations as determined from offshore stations.

3. Results

3.1. Surface Fields

Strong lateral gradients were seen in surface waters between the shelf and the open ocean (Figure 2). Among the most striking were the differences in Conservative Temperature and Absolute Salinity with shelf waters being warmer ($>12.5^\circ\text{C}$) and fresher ($\sim <35.3 \text{ g kg}^{-1}$) than surface waters offshore, which were cooler ($<12.5^\circ\text{C}$) and more saline ($>35.5 \text{ g kg}^{-1}$). A notable gradient in dissolved oxygen concentrations was also evident with lower concentrations on the shelf.

Nutrient concentrations were patchily distributed and variable. Nitrate concentrations were typically 2–4 $\mu\text{mol kg}^{-1}$ on shelf and reached a maximum concentration of $>6 \mu\text{mol kg}^{-1}$ off shelf at station C7, the most northwesterly station sampled. In general, nitrate concentrations increased from south to north and from shelf to ocean. A similar distribution could be seen in the phosphate measurements which increased

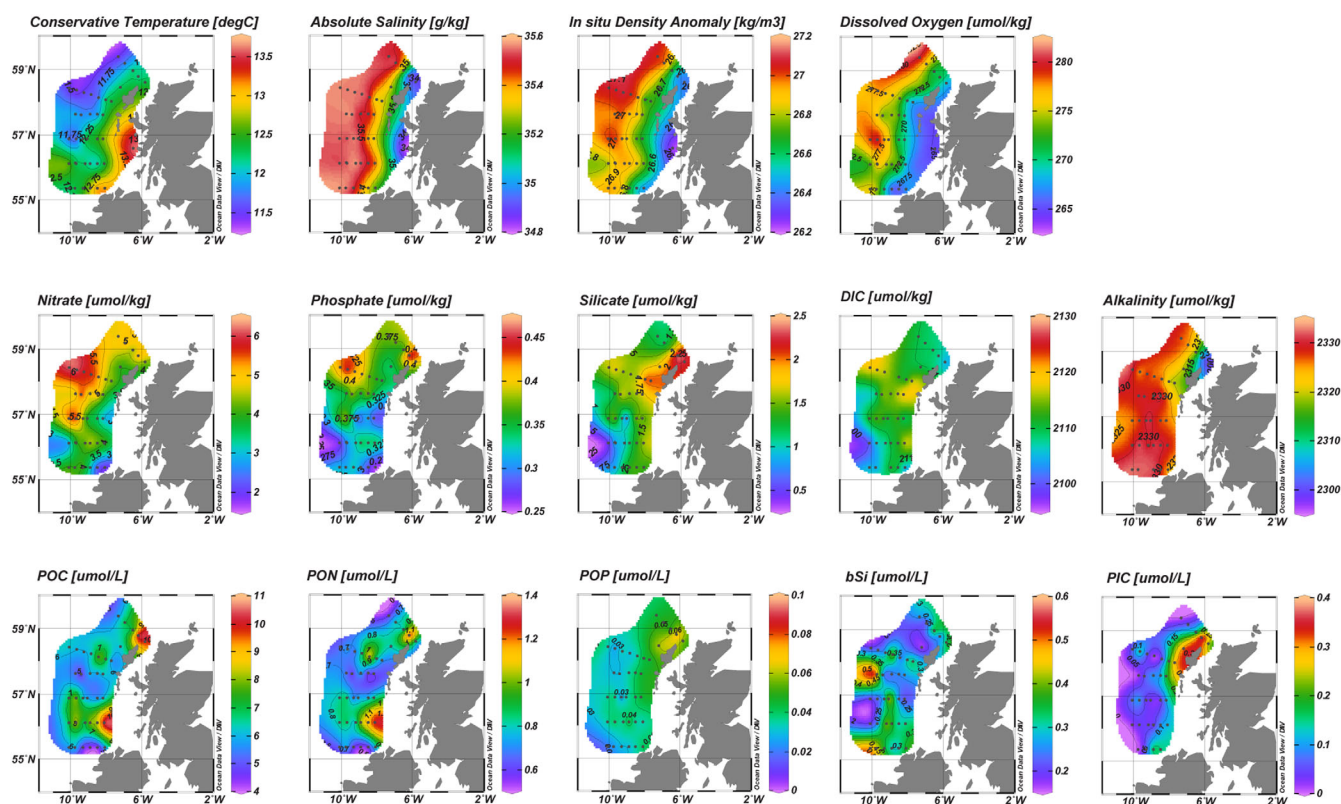


Figure 2. Contoured surface maps (as labeled) showing regional gradients in hydrography, nutrient distributions, and biogenic particulate concentrations.

from south to north but two localized maxima ($>0.4 \mu\text{mol kg}^{-1}$) could be seen in the data, one offshore where concentrations were generally higher and one onshelf which appeared to be linked to the outflow from The Minch, the narrow channel separating the Hebridean Islands from mainland Scotland. Silicate concentrations exceeded $2 \mu\text{mol kg}^{-1}$ at inshore stations close to land but more generally were $\sim 1.5 \mu\text{mol kg}^{-1}$ on the shelf and decreased westward toward the ocean. Variability in DIC concentrations was comparatively muted but higher concentrations were seen across much of the inner shelf. Alkalinity concentrations were $\sim 2325 \mu\text{mol kg}^{-1}$ on shelf, with the exception of those stations around the Isle of Lewis where concentrations were notably lower ($<2315 \mu\text{mol kg}^{-1}$).

The particulate pool concentrations were patchily distributed with the exception of POP and PIC, which exhibited moderate to strong lateral gradients between the innermost stations and outer shelf and offshore stations. Both POP and PIC concentrations were highest around the Isle of Lewis ($\sim 0.06 \mu\text{mol L}^{-1}$ and $>0.3 \mu\text{mol L}^{-1}$ respectively) and rapidly reduced toward the open ocean. POC, PON, and bSi concentrations were heterogeneously distributed with a localized southern maxima along transect F at $\sim 56^\circ\text{N}$ (POC $\sim 10 \mu\text{mol L}^{-1}$, PON $\sim 1.2 \mu\text{mol L}^{-1}$ and bSi $>0.3 \mu\text{mol L}^{-1}$; Figure 2). There was also a suggestion of elevated POC and PON concentrations around the Isle of Lewis to the north, but weaker indications of a comparable peak in bSi concentrations.

3.2. Cross-Shelf Sections

Several of the surface patterns described above extended to the seabed indicating well mixed shelf waters (Figure 3). Benthic water temperatures varied along and between transects, with the warmest waters ($>13^\circ\text{C}$) found along the southernmost transect G. More generally, water temperatures were $>11^\circ\text{C}$ on the shelf, dropping below this at the shelf edge and across the upper continental slope as the depth increased. There was no indication of upwelling at the shelf break (determined by the position of the 9°C isotherm) and examination of the wind direction timeseries for October and November revealed no sustained periods of northerly winds, which are known to induce upwelling in this region [Dickson *et al.*, 1986, 1988].

Absolute Salinities were broadly similar along transects C to G revealing moderate cross-shelf gradients between the lower salinity waters of the inner shelf and the open ocean. Along transect A a strong salinity

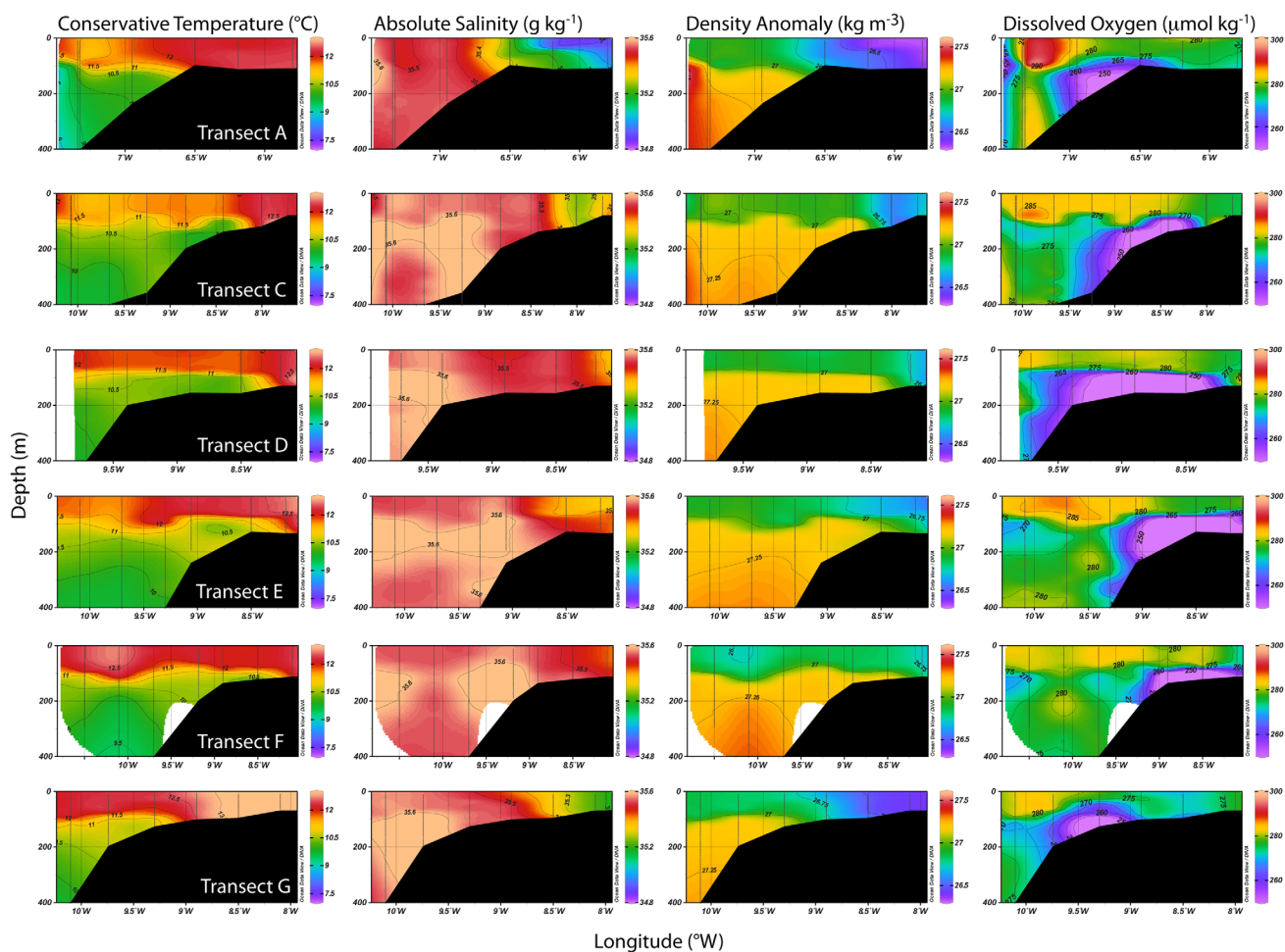


Figure 3. Contoured section plots for each transect of Conservative Temperature, Absolute Salinity, density, and dissolved oxygen concentration.

gradient was observed due to the influence of the inshore Scottish Coastal Current, which reduced Absolute Salinities to $\sim 34.9 \text{ g kg}^{-1}$ at the inner most stations.

The resulting density sections revealed well-mixed shelf waters and waters with variable stratification though there was a clear difference in the proportion of shelf-like (warmer and fresher) and ocean-like (cooler and more saline) stations along each transect with transects A, C, and G revealing more shelf-like conditions at their eastern extremities compared to the other transects.

Dissolved oxygen concentrations did not mirror the pattern seen in surface waters and a pronounced reduction in oxygen concentrations was observed with depth and along each transect at the seabed (Figure 3). At their lowest, oxygen concentrations were $< 250 \text{ } \mu\text{mol kg}^{-1}$, a reduction of $\sim 30 \text{ } \mu\text{mol kg}^{-1}$ with respect to typical surface concentrations and indicative of moderate microbial activity. The spatial extent and volume of the low oxygen region varied along each transect, being broadest along transect D and narrowest on transect G. Inshore stations were generally comparatively well oxygenated at depth, most likely due to shallow water column depths and deep mixing. The bolus of water with reduced oxygen concentrations was typically located between 100 and 400 m depth thus linked the outer shelf and upper continental slope.

As a result of both primary production in surface waters removing DIC, and respiratory processes in the deeper waters of the shelf and upper slope releasing DIC, a strong vertical gradient in DIC concentrations between surface waters and deeper waters on the shelf was evident (Figure 4). DIC concentrations reached local maximum concentrations at the seabed and within the oxygen minimum regions with concentrations

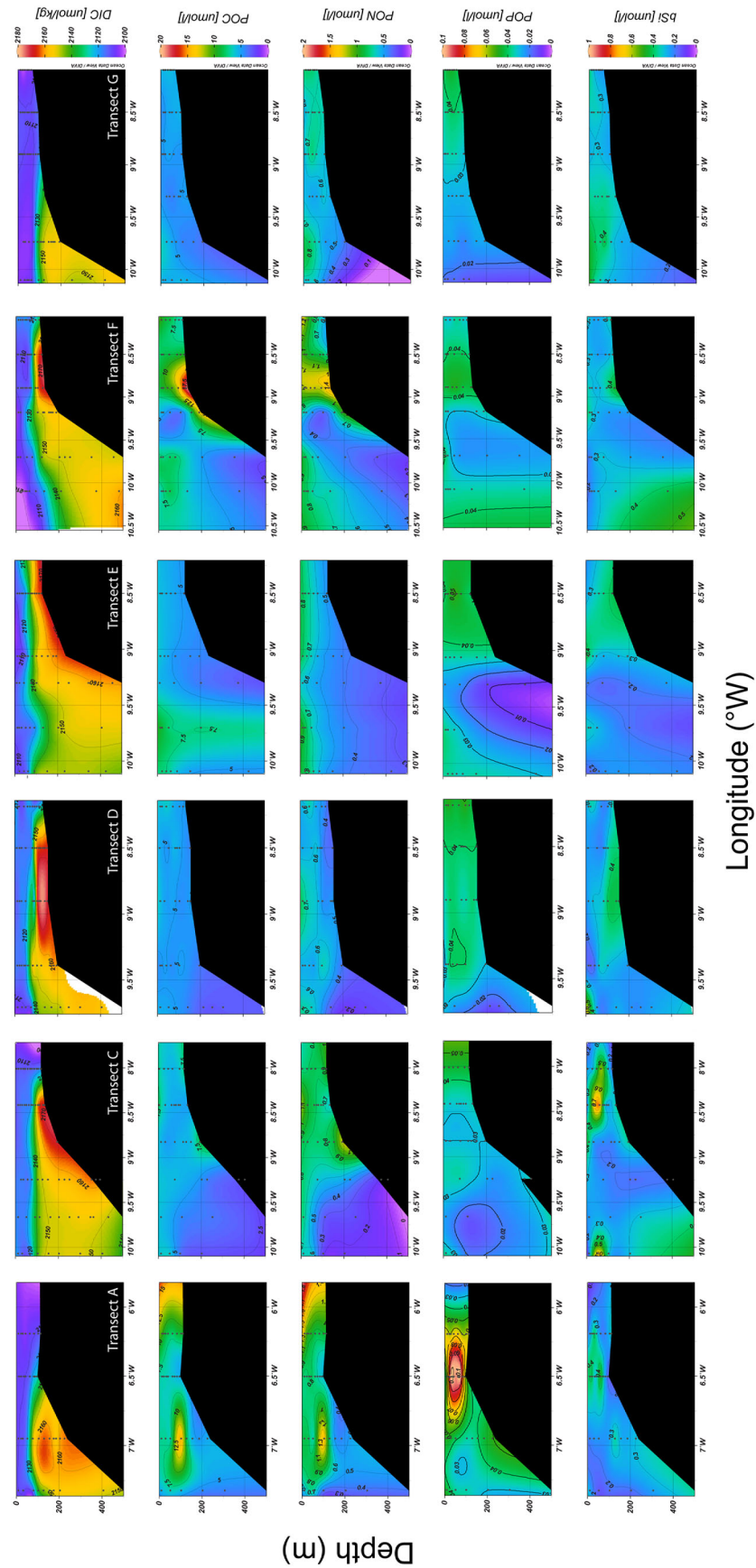


Figure 4. Contoured section plots for each transect of dissolved inorganic carbon (DIC), particulate organic carbon (POC), particulate organic nitrogen (PON), particulate organic phosphorus (POP), and biogenic silica (bSi).

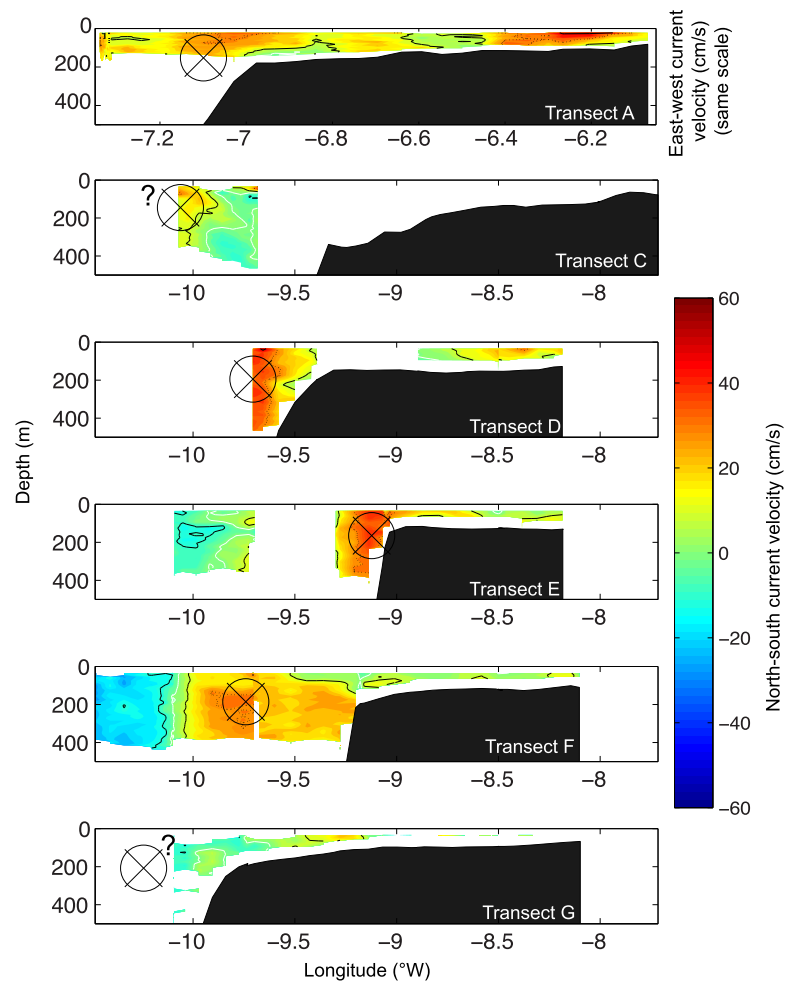


Figure 5. Vessel Mounted Acoustic Doppler Current Profiler measurements of meridional (or zonal) current components along each transect. The position, or assumed position, of the Slope Current is indicated on each plot by the crosshairs.

increasing from 2100 to 2120 $\mu\text{mol kg}^{-1}$ in the upper 100 m to $>2145 \mu\text{mol kg}^{-1}$ below 100 m, a typical increase of at least 25–40 $\mu\text{mol kg}^{-1}$. Maximum near bed DIC concentrations were $\sim 2170 \mu\text{mol kg}^{-1}$, but more commonly were in the range 2145–2165 $\mu\text{mol kg}^{-1}$. Relative to waters at the same depth offshore the near bed DIC concentrations were around 20 $\mu\text{mol kg}^{-1}$ higher.

Table 1. Summary of Transport Fluxes for Each Transect^a

Transect	Latitude (°N)	Depth-Averaged Current (m s^{-1})	Slope Current		Bottom Ekman Transport ($\text{m}^2 \text{s}^{-1}$)	Cross-Shelf Exchange (Sv)	Surface Ekman Transport ($\text{m}^2 \text{s}^{-1}$)	Cross Shelf Exchange (Sv)
			Volume Transport (Sv)					
A	59.19	0.28	0.19 ^b	1.56	0.80	1.89	0.98	
C	58.22	0.15 ^c		0.46 ^b	0.24 ^b	1.92	0.99	
D	57.62	0.36	1.51	2.68	1.38	2.20	1.13	
E	56.87	0.35	1.56	2.50	1.29	1.99	1.03	
F	56.12	0.28	4 ^b	1.57	0.81	2.15	1.11	
G	55.37	0.19	0.53	0.74	0.38	2.07	1.07	
Mean (\pm stdev)		0.29 \pm 0.07 ^c	See Table 5	1.81 \pm 0.79 ^c	0.93 \pm 0.41 ^c	2.04 \pm 0.12	1.05 \pm 0.06	

^aNote that the corresponding cross-shelf exchanges (in Sv; $= 1 \times 10^6 \text{ m}^3 \text{ s}^{-1}$) are calculated by scaling individual transport estimates to the full extent of the Hebrides Shelf edge.

^bLow confidence.

^cDepth-averaged current velocities, bottom Ekman transport and cross-shelf exchange estimates along transect C are incomplete but provided for illustrative purposes only. These results for transect C are not used to calculate the mean values in the bottom row of the table. Note that the surface Ekman transport and the corresponding surface cross-shelf exchange results for transect C are valid and are included in the calculation of the mean values.

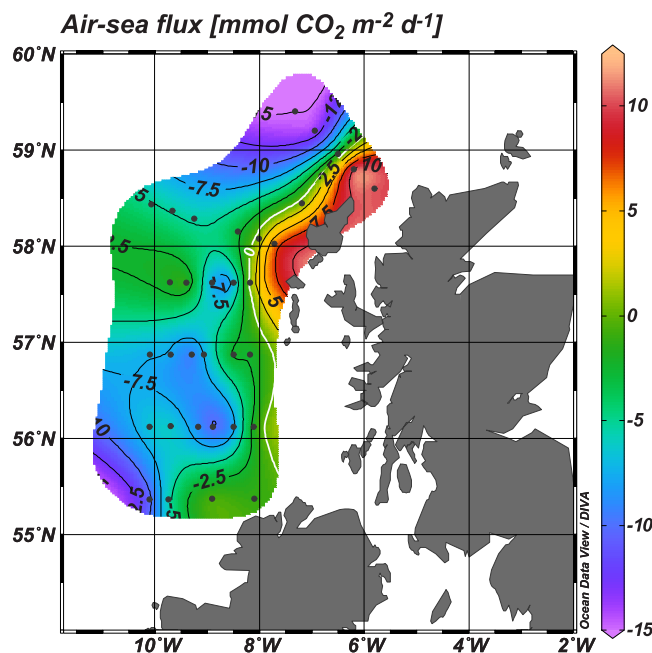


Figure 6. Contoured map of air-sea CO_2 fluxes ($\text{mmol CO}_2 \text{ m}^{-2} \text{ d}^{-1}$) based on calculations described in the text. The zero flux contour is indicated by the white line. Note that positive fluxes signify a flux from the ocean to the atmosphere (outgassing).

tions, POP distributions were also less variable than either POC or PON concentrations. The concentration of bSi was generally $0.2\text{--}0.4 \mu\text{mol L}^{-1}$ close to the seabed, but was consistently elevated on transect D ($\sim 0.4 \mu\text{mol L}^{-1}$). There was a suggestion of elevated bSi concentrations at depth offshore compared to inshore stations.

3.3. Circulation Across the Shelf and Slope Current

VM-ADCP data clearly captured the Slope Current and the contrast between shelf and open ocean waters despite the patchy data coverage (Figure 5). The core of the Slope Current was captured along transects D, E, and F but it is less clear if the current was observed along transect G where the current was either comparatively weak and located at $\sim 9.3^\circ\text{W}$ or located beyond the western end of our transect. In the following, we have assumed that the current was at 9.3°W . On transect C, there is also a question mark over the position of the current given the limited data available for this transect. It is possible that the current was located between 9°W and 9.5°W or $>10^\circ\text{W}$ given its position on other transects. If the latter possibility was true then we may just have resolved the eastern edge of the current at $\sim 10^\circ\text{W}$, but given the apparent strengthening of the Slope Current toward the north it seems more likely that the Slope Current was not resolved on transect C. Along transect A, the Slope Current was located above the 500 m bathymetric contour but we also observed a strong inshore current related to outflow from The Minch. Maximum depth-averaged meridional current velocities ranged from 0.19 to 0.36 m s^{-1} (Table 1). To the west of the Slope Current on transects E and F, there was evidence to suggest a southerly flow, while on the shelf to the east of the Slope Current northerly velocities were weaker and typically $<0.2 \text{ m s}^{-1}$.

3.4. Air-Sea CO_2 Flux

Except for inshore stations immediately around the Isle of Lewis, the Hebrides Shelf was undersaturated in CO_2 with respect to the atmosphere with most pCO_2 values below $380 \mu\text{atm}$. Air-sea CO_2 fluxes ranged from -14.6 to $12.4 \text{ mmol C m}^{-2} \text{ d}^{-1}$ (Figure 6). Six stations indicated positive air-sea CO_2 fluxes (i.e., outgassing to the atmosphere). All six stations were closely grouped, clustered around the Isle of Lewis, and in shallow water. These six stations represented a subregional cluster indicative of important differences in CO_2 dynamics due to a localized mixing/circulation regime. Of these six stations, stations A1 and A2 were notable for low salinities ($<35 \text{ g kg}^{-1}$) and low alkalinities, characteristic features indicating that these two stations were located in the outflow of the Scottish Coastal Current that flows northward through The Minch. The other four stations with positive air-sea CO_2 fluxes (B1, C1, C2, and D1) generally had lower absolute

The distribution of particulate pools was equally patchy with depth as it was in surface waters. With the exception of transect F which revealed elevated POC, PON, and POP concentrations at the shelf break, particulate concentrations reduced with depth and from inshore to offshore. It is possible that sediment resuspension at the shelf break explains the elevated concentration seen on transect F. Concentrations of POC were broadly comparable between transects with typical concentrations of $5\text{--}7.5 \mu\text{mol L}^{-1}$ present at depth over the shelf. Vertical gradients in PON concentration were more obvious between surface waters and those at depth but near seabed concentrations were generally $>0.4 \mu\text{mol L}^{-1}$. POP concentrations were $<0.04 \mu\text{mol L}^{-1}$ and there was a tendency for elevated concentrations close to the shelf break on several transects. Perhaps because of lower concentra-

Table 2. Summary of Cross-Shelf Particulate Silica (bSi) as Weight of Opal (SiO₂·0.4 H₂O), organic Phosphorous (POP), and Organic Nitrogen (PON) Fluxes for the Hebrides Shelf (~55.4–59.2°N) as Calculated in This Study

Transect	Surface Ekman Flux (onshore)			Bottom Ekman Flux (offshore)		
	bSi (kg opal m ⁻¹ d ⁻¹)	POP (kg P m ⁻¹ d ⁻¹)	PON (kg N m ⁻¹ d ⁻¹)	bSi (kg opal m ⁻¹ d ⁻¹)	POP (kg P m ⁻¹ d ⁻¹)	PON (kg N m ⁻¹ d ⁻¹)
A	2.21	0.21	1.28	2.84	0.18	1.06
C	3.66	0.24	1.58	0.97	0.04	0.75
D	4.96	0.26	1.81	3.90	0.17	1.31
E	2.70	0.23	1.76	4.32	0.18	1.47
F	3.24	0.28	2.05	2.25	0.06	2.49
G	4.33	0.16	1.51	1.19	0.02	0.28
Mean (±stdev)	3.52 (1.02)	0.23 (0.04)	1.66 (0.27)	2.90 (1.26)	0.12 (0.07)	1.32 (0.80)

salinities ($\sim < 35.3 \text{ g kg}^{-1}$) compared to stations further offshore ($> 35.4 \text{ g kg}^{-1}$) suggesting that they too were predominately influenced by inshore waters, possibly by terrestrial inputs and by part of the bifurcated Scottish Coastal Current that flows west of the Hebrides [McKay *et al.*, 1986; Inall *et al.*, 2009]. More importantly, however, these stations were in shallow water and the water column was fully mixed. Collectively, the data set revealed important regional gradients in the flux of CO₂ and in general inshore stations were weak CO₂ sinks (or CO₂ sources) whereas outer shelf and open ocean stations were stronger sinks.

Averaged in total or by region, the overall conclusion was that the region was a weak to moderate CO₂ sink. The cruise mean CO₂ sink (using all data) was $-3.98 \text{ mmol C m}^{-2} \text{ d}^{-1}$, whereas the Hebrides region (i.e., all stations inside the boundary shown in Figure 1) was a slightly weaker sink at $-3.2 \text{ mmol C m}^{-2} \text{ d}^{-1}$. The seven stations west of the outer boundary, and therefore reflective of the open ocean were stronger CO₂ sinks with an average flux of $-6.7 \text{ mmol C m}^{-2} \text{ d}^{-1}$. Thus to first order, the open ocean was approximately 2-fold stronger as a CO₂ sink than the shelf at this time and consequently a shelf to ocean gradient in the CO₂ sink can be inferred. The subregional cluster of stations around the Isle of Lewis with positive air-sea fluxes had an average outgassing flux of $5.3 \text{ mmol C m}^{-2} \text{ d}^{-1}$.

To obtain a regional air-sea CO₂ flux, we used the mean Hebrides flux ($-3.2 \text{ mmol C m}^{-2} \text{ d}^{-1}$) and an estimate for the spatial extent of the shelf covered by the survey (54,747 km²) to produce a regional CO₂ sink estimate of $-0.0021 \pm 0.0044 \text{ Tg C d}^{-1}$. The large standard deviation associated with this mean regional flux was due to the inclusion of those stations with a positive air-sea CO₂ flux around the Isle of Lewis. Exclusion of those stations resulted in a mean daily flux of $-5.8 \text{ mmol C m}^{-2} \text{ d}^{-1}$ and a regional flux of $-0.0038 \pm 0.0030 \text{ Tg C d}^{-1}$, suggesting that the outer shelf was most likely a stronger sink than inferred initially.

3.5. Shelf Edge Exchange

Estimates of transport based on maximum depth-averaged currents along each transect are presented in Table 1. Offshore transports associated with the Ekman drain ranged from 0.74 to 2.68 m² s⁻¹, with a mean value of $1.81 \pm 0.79 \text{ m}^2 \text{ s}^{-1}$. The corresponding downslope volume transports ranged from 0.38 to 1.38 Sv with a mean of $0.93 \pm 0.41 \text{ Sv}$. As both the transport and volume transport estimates are sensitive to the magnitude of the depth-averaged current our estimates should be considered as upper limits as we used maximum depth-averaged current speeds in the above calculations due to the poor resolution of the current along some transects preventing calculation of a true mean current velocity. Similarly, we have not accounted for any variation in current strength with depth, which may also lead to an overestimation of current speeds and hence transports.

Also shown in Table 1 are estimates for the wind-driven surface (onshore) flux. Ekman transports ranged from 1.89 to 2.2 m² s⁻¹ with an average transport of $2.00 \pm 0.12 \text{ m}^2 \text{ s}^{-1}$. The corresponding volume transports when scaled to the extent of the Hebrides Shelf edge (516 km) ranged from 0.98 to 1.13 Sv, with a mean of $1.05 \pm 0.06 \text{ Sv}$. The mean onshore surface flux of 1.05 Sv was therefore 13% larger than the mean offshore flux via the Ekman drain (0.93 Sv). Note, however, that on transects D and E the off-shelf flux via the Ekman drain exceeded the surface wind-driven onshore flux, thus the larger overall mean surface flux does not adequately portray dominance of this flux term along all sectors of the Hebrides Shelf. As we cannot fairly extrapolate our results to an annual timescale, this also means that the temporally localized

Table 3. Summary of Cross-Shelf Carbon Fluxes for the Hebrides Shelf (~55.4–59.2°N) as Calculated in This Study^a

Transect	Surface Ekman Flux (onshore) ^b							Bottom Ekman Flux (offshore) ^c							
	DIC (tonnes C m ⁻¹ d ⁻¹)	POC (kg C m ⁻¹ d ⁻¹)	PIC (g C m ⁻¹ d ⁻¹)	DOC (tonnes C m ⁻¹ d ⁻¹)	Total (tonnes C m ⁻¹ d ⁻¹)	%Org (%)	%Inorg (%)	DIC (tonnes C m ⁻¹ d ⁻¹)	POC (kg C m ⁻¹ d ⁻¹)	PIC (g C m ⁻¹ d ⁻¹)	DOC (tonnes C m ⁻¹ d ⁻¹)	Total (tonnes C m ⁻¹ d ⁻¹)	%Org (%)	%Inorg (%)	DICxs (kg C m ⁻¹ d ⁻¹)
A	4.05	12.07	11.20	0.12	4.18	3.27	96.73	3.41	9.52		0.22	3.64	6.31	93.69	31.56
C	4.11	12.22	169.83	0.13	4.25	3.25	96.75	1.01	4.25		0.06	1.08	6.41	93.59	9.31
D	4.69	12.09	21.06	0.14	4.84	3.23	96.77	5.85	11.05		0.38	6.24	6.24	93.76	54.22
E	4.26	14.93	135.05	0.13	4.40	3.31	96.69	5.44	12.14	1119.67	0.35	5.80	6.29	93.71	50.58
F	4.57	17.12	66.77	0.14	4.73	3.34	96.66	3.42	28.37		0.22	3.67	6.82	93.18	31.76
G	4.42	12.17		0.14	4.57	3.25	96.75	1.61	2.66	79.67	0.10	1.71	6.25	93.75	14.97
Mean (±stdev)	4.35 (0.26)	13.43 (2.13)	80.78 (69.79)	0.13 (0.01)	4.50 (0.26)	3.28 (0.043)	96.72 (0.004)	3.94 (1.72)	12.75 (9.48)	599.7 (735.4)	0.26 (0.11)	4.21 (1.84)	6.38 (0.244)	93.62 (0.244)	36.62 (15.99)

^aNote the change in units.

^bThe surface Ekman flux is not affected by the patchy ADCP sampling and results from transect C are used in the calculation of mean surface fluxes presented in the last row of the table.

^cBottom Ekman flux estimates (the "Ekman Drain") along transect C are incomplete but provided for illustrative purposes only. Results from transect C are not used to calculate the mean bottom fluxes in the last row of the table.

dominance of the onshore flux over the offshore flux does not contradict more comprehensive analyses showing a mean downwelling flux in this region [Holt *et al.*, 2009].

To estimate particulate export fluxes, the particulate pool concentrations (Figure 4) were first converted to their respective molar masses. PON, POP, and bSi-opal fluxes varied significantly between transects, with 9-fold variability in PON, 8-fold variability in POP, and 4-fold variability in bSi-opal fluxes. Mean offshore particulate fluxes of $1.32 \pm 0.8 \text{ kg N m}^{-1} \text{ d}^{-1}$, $0.12 \pm 0.07 \text{ kg P m}^{-1} \text{ d}^{-1}$, and $2.9 \pm 1.26 \text{ kg opal m}^{-1} \text{ d}^{-1}$ were derived from the individual transect results (Table 2).

The concentration of POC near the seabed at shelf break stations ranged 4-fold from 42 to 209 mg m^{-3} with a mean concentration of 89 mg m^{-3} . Between each transect POC fluxes could vary significantly due to differences in both the transport term and the POC concentration measured at the shelf break. Consequently, our estimates of cross-shelf POC flux ranged from $2.7 \text{ kg C m}^{-1} \text{ d}^{-1}$ (based on transect G) to $28.4 \text{ kg C m}^{-1} \text{ d}^{-1}$ (based on transect F) highlighting the importance of small-scale heterogeneity in the cross-shelf export of material latitudinally along the shelf edge (Table 3). The product of the mean Ekman drain transport ($1.81 \text{ m}^2 \text{ s}^{-1}$) and the mean POC concentration ($89 \pm 63 \text{ mg m}^{-3}$) was an export flux of POC from the shelf to the continental slope and open ocean of $13.9 \text{ kg C m}^{-1} \text{ d}^{-1}$, slightly larger than the true mean derived from the individual transects of $12.8 \text{ kg C m}^{-1} \text{ d}^{-1}$ (Table 3) due to spatial variability, or if scaled to the extent of the Hebrides Shelf edge, a total off-shelf POC flux of $0.007 \pm 0.005 \text{ Tg C d}^{-1}$.

Deep-water PIC measurements were limited and the few available observations indicate PIC concentrations of between 1.3 and 7.2 mg C m^{-3} near the seabed (note that here we refer to weights of PIC as carbon not calcite). The mean concentration was $4.1 \pm 2.6 \text{ mg C m}^{-3}$ ($n = 4$) for samples collected over a depth range of 107–193 m. Based on this mean value and using the mean bottom Ekman transport term (Table 1), we estimate a mean export of $0.64 \text{ kg C m}^{-1} \text{ d}^{-1}$. However, two of the four samples were collected at $\sim 190 \text{ m}$ depth (1.3–5.2 mg C m^{-3}) providing a lower mean value of $3.2 \pm 2.8 \text{ mg C m}^{-3}$ that may be more appropriate for evaluating the shelf export flux and which resulted in a lower export flux of $0.5 \text{ kg C m}^{-1} \text{ d}^{-1}$. Both approximations are similar to the true mean of $0.6 \text{ kg C m}^{-1} \text{ d}^{-1}$ derived from the individual transects (Table 3), but fail to adequately portray the 14-fold variability in the flux between transects. The export of carbon as PIC from the shelf via the Ekman drain was therefore an order of magnitude smaller than the export of carbon as POC. This may in part reflect the offshore position of most coccolithophore blooms in this region [Holligan, 1986], which may limit sinking and deposition of PIC on the shelf.

Following similar arguments to the above, it is possible to estimate the offshore transport of DIC. We assessed this in two ways, first by using the total DIC concentration and second by defining an excess concentration relative to offshore waters to reflect the accumulation of DIC in the deeper waters of the shelf. Total offshore fluxes of DIC ranged from 1.61 to 5.85 tonnes $\text{C m}^{-1} \text{ d}^{-1}$ by transect and averaged $3.94 \pm 1.72 \text{ tonnes C m}^{-1} \text{ d}^{-1}$ (Table 3). In contrast, and by using a typical excess of $20 \mu\text{mol kg}^{-1}$ as indicative of the difference between near bed DIC concentrations on shelf (source region) relative to open ocean waters at the same depth (receiving region), rather than the surface to seabed difference, we estimate that the Ekman drain could transport an excess of $0.037 \pm 0.016 \text{ tonnes C m}^{-1} \text{ d}^{-1}$ from the Hebrides Shelf to the open ocean. By transect the excess DIC flux ranged from 0.015 to 0.054 tonnes $\text{C m}^{-1} \text{ d}^{-1}$ (Table 3).

We also estimated the onshore fluxes in the surface Ekman layer using mean mixed layer concentrations calculated from offshore stations on each transect. Onshore bSi-opal fluxes ranged from 2.2 to 5.0 (mean 3.5 ± 1.0) $\text{kg opal m}^{-1} \text{ d}^{-1}$, PON fluxes ranged from 1.3 to 2.1 (mean 1.7 ± 0.3) $\text{kg N m}^{-1} \text{ d}^{-1}$, and POP fluxes ranged from 0.16 to 0.28 (mean 0.23 ± 0.04) $\text{kg P m}^{-1} \text{ d}^{-1}$ (Table 2). Similarly, total onshore DIC fluxes ranged from 4.05 to 4.69 tonnes $\text{C m}^{-1} \text{ d}^{-1}$, and averaged $4.35 \pm 0.26 \text{ tonnes C m}^{-1} \text{ d}^{-1}$. POC fluxes ranged from 12.1 to 17.1 $\text{kg C m}^{-1} \text{ d}^{-1}$, and averaged $13.4 \pm 2.1 \text{ kg C m}^{-1} \text{ d}^{-1}$. PIC fluxes were considerably smaller and ranged from 11.2 to 169.8 $\text{g C m}^{-1} \text{ d}^{-1}$ with an average of $80.8 \pm 69.7 \text{ g C m}^{-1} \text{ d}^{-1}$ (Table 3).

These results reinforce the importance of recognizing spatial heterogeneity in the export or import of material along the shelf break. They also reveal that the total offshore POC flux was approximately 3 times larger than the mean air-sea influx of CO_2 , that the PIC flux was comparatively small compared to both POC and CO_2 fluxes and that all particulate carbon fluxes were small compared to the offshore flux of DIC. However, dissolved organic carbon (DOC) represents the second largest reservoir of carbon in the ocean and before discussing a tentative carbon budget for this region we include in Table 3 estimates of surface and deep DOC fluxes based on representative DOC concentrations obtained from the global synthesis of *Barron and*

Table 4. Literature Observations of the Slope Current Between ~55°N and ~60°N^a

Latitude (°N)	Slope Current Velocity (m s ⁻¹)	Slope Current Volume Transport (Sv)	Notes	Reference
59	0.3	1.7	Mean current	Huthnance [1986]
58	0.15	1.5		
56	0.06			
57.1	0.16	0.5	Current meter	<i>Booth and Ellett</i> [1983]
60.22	0.77		Current meter (maximum hourly mean)	
60.21	0.62			
60.17	0.87			
59.78	0.78			
59.66	0.81			
59.14	0.52			
59.09	0.78			
58.14	0.47			
58.11	0.56			
58.01	0.50			
57.94	0.66			
57.35	0.52			
57.31	0.46			
56.6		1.6	Model estimate	<i>Holt et al.</i> [2009]
60	0.30			<i>Huthnance and Gould</i> [1989]
54.5	0.10		Current meter	<i>White and Bowyer</i> [1997]
55.04	0.22		Current meter	
56.48	0.15	2	ADCP mooring	<i>Souza et al.</i> [2001]
59.5		1.7	VMADCP	<i>Chafik et al.</i> [2014]
57		1.8	Geostrophy	<i>Holliday et al.</i> [2015]

^aSee also Table 5.

Duarte [2015] for comparison. Note that while our usage of the typical mean DOC concentrations for open ocean (63 μmol L⁻¹) and shelf waters (139 μmol L⁻¹) reported by *Barron and Duarte* [2015] results in the transect to transect variability being governed by the variability in the transport term alone, the apparent magnitude of these fluxes should be correct.

4. Discussion

4.1. CO₂ Fluxes

Air-sea CO₂ fluxes vary regionally and seasonally, and in temperate shelf sea systems are strongly influenced by biological productivity, local mixing regimes, and prevailing wind speeds. Recent efforts to constrain global air-sea CO₂ fluxes in coastal seas highlight important seasonality and latitudinal variability [*Chen et al.*, 2013; *Laruelle et al.*, 2014]. Our temporally limited observational data set is therefore unlikely to provide a firm quantitative basis for calculating an annual flux for the Hebrides Shelf or more broadly for the NW European Shelf. Nevertheless, our mean daily air-sea CO₂ flux of -3.2 mmol C m⁻² d⁻¹, is similar to a mean daily estimate of -3.5 mmol C m⁻² d⁻¹ derived from the mean annual estimate of -1.29 mol C m⁻² yr⁻¹, reported for the NW European Shelf by *Laruelle et al.* [2014]. Our results may not therefore be significantly seasonally biased relative to the annual mean for the NW European Shelf and may also therefore be more broadly representative of the autumn season (~September-December) rather than just the observation period (late October-Early November).

The annual CO₂ sink across the NW European Shelf has been estimated as -17.165 Tg C yr⁻¹ [*Laruelle et al.*, 2014]. By crudely extrapolating the regional daily air-sea CO₂ flux obtained in this study (-0.0021 Tg C d⁻¹) to a full year, we estimate that the annual sink in this region would have been -0.77 Tg C yr⁻¹, or 4.5% of the entire NW European Shelf sink term estimated by *Laruelle et al.* [2014]. As defined, the extended Hebrides Sea Region of 54,747 km² represents 4.9% of the area of the NW European Shelf (1112 × 10³ km²), suggesting that the Hebrides Shelf was broadly representative of mean conditions across the NW European Shelf. However, this is based on the extrapolation of autumnal measurements across a full year and does not include the effects of seasonality and biological productivity, both of which are significant, so this calculation is only a qualitative indicator at best. It does however suggest that the Hebrides Shelf was broadly typical of the wider region and was neither an unseasonably strong sink nor source for CO₂ during autumn 2014.

Table 5. Interannual Estimates of Slope Current Volume Transport and Depth-Averaged Currents From Selected Extended Ellett Line Cruises at 57°N During October in Comparison to Results From This Study

Cruise Identifier	D223	CD176	D312	DY017 (this study)
Date	Oct 1996	Oct 2005	Oct 2006	Oct–Nov 2014
Latitude (°N)	57.06°N	56.8°N	57°N	55.4–57.6°N ^a
Max VMADCP depth penetration (m)	400	275	350	400
Current width (km)	37	76	19	35–57
Depth avg current (m s ⁻¹)	0.3	0.50	0.16	0.19–0.36
Volume transport (Sv)	1.06	1.48	0.53	0.53–1.56 ^b

^aNote that these summary values do not include information from transects A or C of the present study due to limitations within the data on these transects.

^bVolume transport estimate of 4 Sv obtained from transect F of the present study (Table 1) excluded due to the distorting influence of a cyclonic eddy on this transect.

However, intraregional variability in the sign of the air-sea CO₂ flux, and recognition that inner and outer shelf regions vary significantly in their ability to absorb/release CO₂ [e.g., *Chen et al.*, 2013] can have a significant impact on the representative nature of our results.

4.2. Slope Current

The Hebrides Shelf region, and in particular the Slope Current, have been the focus of several previous studies. In Table 4, we present literature observations of Slope Current velocities and/or volume transports measured using various methodologies. It reveals significant variability between studies conducted at different latitudes, and between studies conducted in different years, supporting previous conjecture that there is substantial variability in the Slope Current in this region. Nevertheless, the majority of our observations (Table 1) lie within the range of previous observations (Table 4).

The Extended Ellett Line (EEL) has sampled the shelf and slope areas at ~57°N at least annually since 1975 [*Holliday and Cunningham*, 2013; *Holliday et al.*, 2015]. The majority of EEL cruises were conducted in spring or summer with far fewer cruises conducted in autumn and almost none in winter. Nevertheless, EEL cruises in 1996 (D223), 2005 (CD176), and 2006 (D312) were conducted in October and the VMADCP data from these cruises allows for a comparative study to the observations we report here. In Table 5, we summarize our main findings. Despite crossing the shelf at similar latitudes (due to fixed station positions), there is considerable variability in the appearance of the Slope Current in the EEL cruise data sets. For example, the apparent width of the current varied almost 4-fold from 19 km at its narrowest (October 2006) to 76 km at its widest (October 2005). While latitudinal variability in the Slope Current width was recognized by *Dickson et al.* [1986], there appears to be limited description in the literature of changes in Slope Current width on interannual timescales. Similarly, but to a smaller extent, the depth-averaged current velocities varied over 2-fold between observation periods with the strongest observed current of 0.49 m s⁻¹ occurring during the period of widest current (October 2006). The variability in both current width and depth-averaged current velocities also impacts the apparent volume transport associated with the current, which ranged from 0.53 to 1.48 Sv. Such transport estimates are in keeping with other independent estimates of the current transport, and our new observations, but the acoustic penetration of the VMADCP also impacts the accuracy of these estimates. As there is considerable variability in the depth to which the current was resolved on each EEL cruise, varying from 275 to 400 m, the apparent volume transports are susceptible to several errors (the same is true of our results). It is, however, reassuring that approximately the same magnitude for the Slope Current volume transport can be obtained from different VMADCP data sets collected over an 18 year period (1996–2014). Nevertheless, the long-term mean geostrophic volume transport calculated by *Holliday et al.* [2015] from mean EEL hydrographic profiles across the Rockall Channel indicated a larger mean volume transport of 1.8 ± 0.4 Sv associated with the Slope Current, which suggests that direct observation of the Slope Current by VMADCP underestimates the true transport (though note that the geostrophic estimate is itself biased by the seasonal distribution of EEL cruises). In light of the mean geostrophic transport estimate, comparable estimates of the volume transport from EEL cruises and from the literature, the unusually high transport estimate of 4 Sv calculated for transect F (Table 1) looks increasingly anomalous. At the western end of transect F (Figure 5), there was a strong southerly flow which in conjunction with equally strong northerly flows to the immediate east (~9.8°W) most likely signified the presence of a cyclonic eddy along the western edge of the current, thus biasing our volume transport estimates for this transect.

Table 6. Literature Estimates of Offshelf Exchange Via the Ekman Drain Along the West Scotland Shelf

Latitude (°N)/region	Transport (m ² s ⁻¹)	Volume transport (Sv)	Reference
54–57°N	1.75	~0.6	Holt and Proctor [2008]
~53–63°N		0.13–0.28	Holt et al. [2009]
56.48°N	1.6	0.83	Simpson and McCandliss [2013]
56.48°N	0.46	0.3	Souza et al. [2001]
W. Scotland Shelf		~0.52	Huthnance et al. [2009]
Western shelf ~52–60°N		1.15	Wakelin et al. [2012]
Hebrides Shelf ~55–59°N	1.81	0.93	This study

Confirmation of this was found in satellite altimetry data, which revealed a sea level anomaly consistent with a cyclonic eddy, centered just north of the midway point between stations F5 and F6.

4.3. Surface Ekman Fluxes

Our surface wind-driven Ekman fluxes appear larger than typical flux estimates reported in the literature, which are often based on annually averaged data (e.g., 1.17 m² s⁻¹; Huthnance, 2010). Significant seasonal variability in the surface Ekman flux term is recognized however and when viewed in this context our average transport of 2.04 ± 0.12 m² s⁻¹ (Table 1) is not too dissimilar to the mean winter value of 1.73 m² s⁻¹ reported by Huthnance et al. [2009] or the mean annual value of 1.71 m² s⁻¹ derived from the results of Wakelin et al. [2012]. There is also the possibility that wind speeds and wind directions during October–November 2014 were favorable for onshore transport. The region experiences prevailing westerly winds and during the observation period strong southerly winds were dominant and these may have enhanced the onshore surface flux, particularly as the Hebrides Shelf is broadly orientated north-south.

4.4. Ekman Drain and Fluxes

Our estimates of the offshelf downslope transport via the Ekman drain (Table 1) are similar to the few previous estimates available for this shelf (Table 6). This is largely due to the broad consistency of Slope Current velocities between studies (Table 4). For example, Simpson and McCandliss [2013] reported peak Slope Current velocities of 0.3 m s⁻¹ at 56.47°N, and a mean Ekman drain transport of 1.6 m² s⁻¹, which if scaled to the Hebrides Shelf (516 km) would translate to a total volume transport of 0.83 Sv. Our new observations compare well to these measurements with a mean transport of 1.81 m² s⁻¹ and mean volume transport of 0.93 Sv (Table 6). Aside from model based estimates, which represent the majority of previous attempts to quantify the Ekman drain, the only other direct observation we have identified by Souza et al. [2001] indicated a lower transport of 0.46 m² s⁻¹ and a volume transport of 0.3 Sv. This almost certainly results from use of a lower current velocity derived from summer observations compared to those measured here (Table 4). Despite these differences results from these observational studies do compare favorably to modeled estimates of the offshelf transports suggesting that the region may be comparatively well represented in numerical models though there is a clear need for additional observations to better constrain these transports (Table 6).

Despite our offshelf downslope transports exhibiting an almost 4-fold variation between transects the mean transport of 1.81 m² s⁻¹ was comparable to the mean estimate of 1.75 m² s⁻¹ obtained by Holt and Proctor [2008] based on a 40 year model run for the region. This suggests that conditions during October–November 2014 were near to (model) mean conditions (i.e., neither strongly enhanced or weakened). However, Xu et al. [2015] describe important seasonal to interdecadal variability in the Slope Current that will impact the variability in downslope transport over similar timescales, which in addition to the 4-fold variability we highlight between transects, suggests that the flux of material offshelf is likely to be highly variable along the shelf break over a range of timescales.

Our estimates of downslope carbon flux are therefore harder to constrain. By scaling the mean offshelf flux of organic carbon (as POC; 12.75 ± 9.48 kg C m⁻¹ d⁻¹) associated with the Ekman drain to the length of the shelf break studied here (516 km) we obtain a total offshelf POC flux of 0.007 ± 0.005 Tg C d⁻¹ which matches the modeled total organic carbon flux of 0.007 Tg C d⁻¹ obtained by Wakelin et al. [2012] for a slightly larger sector of the NW European shelf (~52–60°N; ~1000 km shelf break length). Clearly, extrapolation of our per unit length cross-shelf flux to the same shelf break length used in the Wakelin study would

Table 7. Summary Offshelf Fluxes of Particulate Material Per Unit Area of Shelf^a

Transect	POC (mmol C m ⁻² d ⁻¹)	PON (mmol N m ⁻² d ⁻¹)	POP (mmol P m ⁻² d ⁻¹)	PIC (mmol C m ⁻² d ⁻¹)	bSi-opal (mmol opal m ⁻² d ⁻¹)	CO ₂ flux (mmol C m ⁻² d ⁻¹)
A	7.48	0.71	0.05		0.40	
C	3.34	0.50	0.01		0.14	
D	8.68	0.88	0.05		0.55	
E	9.54	0.99	0.05	0.88	0.60	
F	22.28	1.68	0.02		0.31	
G	2.09	0.19	0.01	0.06	0.17	
Mean (±stdev)	10.01 (7.44)	0.89 (0.54)	0.04 (0.02)	0.47 (0.58)	0.41 (0.18)	-3.2

^aThese estimates are determined by first calculating the total offshelf flux obtained by scaling up the results of Tables 2 and 3 to the length of the shelf break studied here (516 km) and then dividing the total flux by the area of the extended Hebrides Sea Region lying between 55.3°N and 59.2°N (54,747 km²) as shown in Figure 1. We include the mean regional ingassing CO₂ flux for comparison.

effectively double the resulting offshelf POC flux associated with the Ekman drain and greatly exceed the model estimate of total organic carbon flux. While this suggests that differences in organic carbon flux between the observations and the model may be significant we caution against over interpretation of this result as our own observations show the cross-shelf flux to be highly spatially heterogeneous and unlikely to persist at our mean flux rate over large spatial distances or at a fixed value throughout the year. This further suggests that global extrapolations from limited observations may contain significant errors. Nevertheless, both flux estimates are 14-fold larger than the estimate of 0.0005 Tg C d⁻¹ obtained by scaling the single observation of 0.99 kg C m⁻¹ d⁻¹ reported by Simpson and McCandliss [2013] at ~56.5°N to the extent of the Hebrides Shelf edge, suggesting that cross-shelf fluxes of organic carbon remain poorly quantified both observationally and in models. Differences between Simpson and McCandliss [2013] and the present study may be explained given the transport variability between transects reported here, suspected seasonality in such transport terms, and differences in methodologies used for determining POC concentrations (transmissometer/suspended particulate matter relationship versus elemental analysis). Despite such uncertainties our results suggest that downslope POC fluxes are significant compared to air-sea CO₂ fluxes, for example. Our results also imply that the downslope POC flux is probably highly significant for the benthic communities of the continental slope that rely upon a supply of organic carbon from surface waters. At present, and with the data available, it is unclear how this flux and its importance for benthic communities, would vary seasonally, nor over what distance this material would be deposited. Simple calculations assuming an even deposition of the exported POC over the seabed between 200 and 2000 m depth (~50 km distance) suggest an average flux of 0.24 ± 0.18 g C m⁻² d⁻¹ (88 ± 65 g C m⁻² yr⁻¹), somewhat larger than typical benthic respiration rates 0.05 g C m⁻² d⁻¹ (20 g C m⁻² yr⁻¹) assumed for this region [Simpson and McCandliss, 2013]. It is probable that the majority of this material is remineralized within the water column.

Although the offshelf flux of POC represents only ~0.3% of the total offshelf carbon flux, which is dominated by DOC (6.1%) and DIC (93.6%), it is instructive to consider the global significance of the downslope POC flux from the Hebrides Shelf. To do so we compared our results to similar findings from the East China Sea and to a mass balance derived global shelf sea carbon budget. *Chen and Wang* [1999] reported an offshelf downslope POC flux from the East China Sea of 695 × 10⁹ mol C yr⁻¹. This equates to a daily flux of 0.02 Tg C d⁻¹, approximately 3-fold larger than we report for the Hebrides Shelf (0.007 Tg C d⁻¹) despite the East China Sea being ~16-fold larger in area. If we convert both downslope estimates to a per unit area basis using the respective shelf areas we find a mean downslope POC export of 2.1 mmol C m⁻² d⁻¹ for the East China Sea and 10.01 mmol C m⁻² d⁻¹ for the Hebrides Shelf (Table 7). This suggests a stronger export potential for the Hebrides Shelf compared to the East China Sea.

Based on a global synthesis of shelf sea carbon fluxes and a mass balance calculation, *Chen et al.* [2003] estimated a global downslope POC flux of 20 × 10¹² mol C yr⁻¹. Converting this to a daily per unit area flux using a global shelf area of 26 × 10⁶ km we obtain a daily flux of 2.11 mmol C m⁻² d⁻¹. Thus our estimate of the offshelf downslope POC flux of 10.01 mmol C m⁻² d⁻¹ for the Hebrides Shelf is ~5-fold larger than the global mean. However, we urge caution in the interpretation of these comparisons as the offshelf flux of POC from the Hebrides Shelf may integrate over a larger shelf area than we have defined and an increase in shelf surface area would decrease the per unit area flux (i.e., the offshelf flux could include POC from inshore waters or the Irish Sea). Nevertheless, the Hebrides Shelf appears to be a prominent source of POC

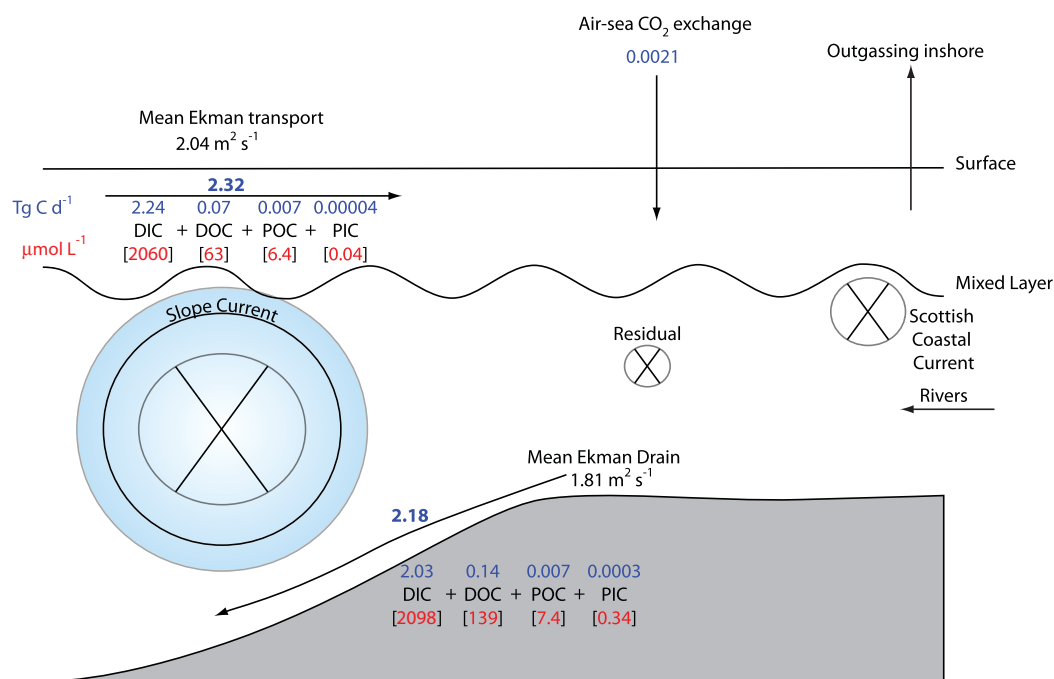


Figure 7. Schematic showing a partial carbon budget and dominant physical circulatory features for the Hebrides Shelf in autumn 2014. Highlighted are the major carbon fluxes associated with the (offshelf) Ekman drain, (onshelf) surface Ekman layer and the mean regional air-sea CO_2 flux as measured in this study. The mean Ekman transports are shown in black ($\text{m}^2 \text{ s}^{-1}$), cross-shelf carbon fluxes are shown in blue (units of Tg C d^{-1}) while mean concentrations of the carbon pools are shown in red ($\mu\text{mol L}^{-1}$). Note that parameter concentrations reported in the text in $\mu\text{mol kg}^{-1}$ were first converted to $\mu\text{mol L}^{-1}$ for the purposes of cross-shelf flux calculations.

with a total offshelf flux ($0.007 \text{ Tg C d}^{-1}$ or $12.75 \text{ kg C m}^{-1} \text{ d}^{-1}$) that represents $\sim 1\%$ of total global down-slope POC export from shelf seas (0.66 Tg C d^{-1} ; based on *Chen et al.* [2003]) despite representing only 0.21% of global shelf sea area.

An alternative calculation based on a global shelf break length of 150,000 km [*Jahnke*, 2010] implies a global mean POC export of $4.38 \text{ kg C m}^{-1} \text{ d}^{-1}$, which implies that the Hebrides Shelf exported 2.9-fold more carbon per meter of shelf break than the global mean, while representing 0.34% of global shelf break length. Thus regardless of either shelf area or shelf break length the Hebrides Shelf is exporting more particulate carbon per unit of measure than the global mean.

The inorganic carbon flux, which dominates the flux of total carbon, was estimated in two ways (Table 3). Under the first approach our total inorganic carbon flux (PIC + DIC excess (DICxs); $36.62 \text{ kg C m}^{-1} \text{ d}^{-1}$ equivalent to $0.019 \text{ Tg C d}^{-1}$) was considerably smaller than the modeled flux of $2.548 \text{ Tg C d}^{-1}$ reported by *Wakelin et al.* [2012]. This was due to our use of the DIC excess in near bottom waters relative to waters at the same depth offshore rather than the absolute DIC concentration to assess the offshelf flux. Repeating this comparison for total DIC content using representative DIC concentrations of 2145–2169 $\mu\text{mol kg}^{-1}$ by transect (Figure 4) we obtained a total inorganic carbon flux (DIC + PIC) of $3.94 \pm 1.72 \text{ tonnes C m}^{-1} \text{ d}^{-1}$ ($2.034 \pm 0.89 \text{ Tg C d}^{-1}$) (Table 3), which was only $\sim 20\%$ smaller than the model flux implying that modeled fluxes of inorganic carbon may be better understood than fluxes of organic carbon.

Based on the calculation of excess DIC, which provides an indication of the net exportable pool of DIC in the benthic layer of the shelf ($36.62 \pm 16.0 \text{ kg C m}^{-1} \text{ d}^{-1}$; $0.019 \text{ Tg C d}^{-1}$), we estimate that the mean air-sea CO_2 flux for the region would have represented 11% of the excess DIC pool compared to only $\sim 1\%$ of the total DIC pool flux.

In Figure 7, we present a provisional carbon budget for the outer Hebrides Shelf region based on total carbon fluxes in both surface and bottom Ekman layers. We have augmented this with estimated fluxes of dissolved organic carbon (DOC) based on the representative DOC concentrations reported by *Barron and Duarte* [2015] of 63 and 139 $\mu\text{mol L}^{-1}$ for open ocean and shelf waters respectively (Table 3). This budget reveals that (i) the mean onshore total carbon flux was 6% larger than the mean offshore total carbon flux

(though the net flux on an individual transect could be onshore or offshore with a net difference of up to $\sim 60\%$; Table 3), (ii) there was a net onshore flux of DIC, driven by the larger surface Ekman flux, despite increased DIC concentrations at depth (though again note the transect to transect variation; Table 3), (iii) there was a net offshore flux of PIC possibly due to resuspended material near the seabed, (iv) assuming that the DOC concentrations are appropriate for the region and time of year, a net offshore flux of DOC, which supports the global analysis of *Barron and Duarte* [2015], and (v) the net flux of POC was approximately 0 (due to rounding) but a small import of POC of $\sim 0.5 \text{ kg C m}^{-1} \text{ d}^{-1}$ may have been more likely (Table 3). We include our regional mean air-sea CO_2 flux, noting that it is highly probable that inshore waters would have contributed to an outgassing of CO_2 at this time given the spatial patterns in our own data (Figure 6) and recent syntheses showing marked differences between inner shelf and outer shelf regions [*Chen et al.*, 2013]. To facilitate comparison of our results with other shelf systems we have also converted the individual offshelf transect particulate fluxes to a per unit area basis based on the shelf area studied (i.e., $54,747 \text{ km}^2$; Table 7). Note that such conversions are sensitive to the choice of area used. Nevertheless, mean particulate fluxes of $10.01 \text{ mmol C m}^{-2} \text{ d}^{-1}$, $0.89 \text{ mmol N m}^{-2} \text{ d}^{-1}$, and $0.04 \text{ mmol P m}^{-2} \text{ d}^{-1}$ for POC, PON, and POP respectively and $0.47 \text{ mmol C m}^{-2} \text{ d}^{-1}$ and $0.41 \text{ mmol opal m}^{-2} \text{ d}^{-1}$ for PIC and bSi-opal fluxes resulted. Based on these mean fluxes, the mean stoichiometric C:Si:N:P content of the exported particulate material was 250:10:22:1. Furthermore, assuming an annual net primary production rate of $200 \text{ g C m}^{-2} \text{ yr}^{-1}$ the annual cross-shelf POC flux associated with the Ekman drain would equate to 22% of annual primary production.

Based on the total carbon flux of 2.32 Tg C d^{-1} ($4.50 \pm 0.26 \text{ tonnes C m}^{-1} \text{ d}^{-1}$), the onshore flux of organic carbon (DOC and POC) represented $\sim 3.3\%$ of the total onshore carbon flux while inorganic carbon (DIC and PIC) represented $\sim 96.7\%$. This compares well to the estimated inorganic carbon content of inflowing waters of 97% reported for the North Sea by *Thomas et al.* [2005]. However, within the offshore flux associated with the Ekman drain (2.18 Tg C d^{-1} or $4.21 \pm 1.84 \text{ tonnes C m}^{-1} \text{ d}^{-1}$) organic carbon represented 6.4% on average with inorganic carbon representing 93.6%. Thus, despite the net flux of carbon being onshore, the offshelf flux of carbon contained a significantly larger organic component than the onshore flux. Within this organic component an average of 95% was represented by dissolved organic carbon and 5% by particulate organic carbon thus demonstrating the significance of dissolved fractions for organic carbon export from coastal seas. Viewed against these larger total carbon fluxes the mean air-sea flux of CO_2 was comparable to 30% of the offshelf POC flux, $\sim 1.4\%$ of the total offshelf organic carbon flux, and $< 0.1\%$ of the total offshelf carbon flux.

How is the offshelf organic carbon flux sustained? It is unlikely that our measured POC flux persists at its measured magnitude year round and indeed models of the NW European Shelf show strong seasonality in carbon fluxes and primary production [*Wakelin et al.*, 2012; *Artoli et al.*, 2014]. It is highly probable therefore that the accumulation of organic matter beneath the mixed layer has a seasonal component to it and that the offshelf fluxes of biogenic material we have calculated are toward upper potential values. We base this assessment on the knowledge that the development of an exportable reservoir of organic material will be linked to the residence time of the shelf, which can be measured in months due to weak residual flows and on established seasonality in the Slope Current which ultimately drives any cross-shelf transport. Globally the mean coastal ocean residence time is ~ 130 days [*Huthnance*, 1995]. In the Hebrides Shelf region monitoring of ^{137}Cs discharges from the Sellafield nuclear reprocessing plant indicate that residence times may be longer, possibly over 1 year [*Prandle*, 1984], and even within identifiable currents such as the Scottish Coastal Current it is estimated to take ~ 9 months for ^{137}Cs to transit from the Irish Sea to the mid-Hebrides Shelf region [*McKay et al.*, 1986; *McCubbin et al.*, 2002]. Long residence times will therefore allow for the retention and accumulation of material from the productive spring and summer months which, if not remineralized upon settling beneath the mixed layer and instead retained within an unconsolidated benthic fluff layer [*Jago et al.*, 1993], may ultimately become entrained into the Ekman drain and exported offshore. Neither the lability or age of the DOC fraction is known and the long-term consequences of a net flux of organic carbon from the shelf to the ocean requires further investigation, a topic previously highlighted by *Barron and Duarte* [2015]. Long residence times, coupled with weak cross-shelf exchange, may also explain two other interesting attributes of our observational data set, specifically the (seasonal) accumulation of excess DIC and the lower oxygen waters seen beneath the mixed layer over extensive sections of the shelf; features which although common for the NW European Shelf nevertheless require time and quiescent conditions to form within.

4.5. Limitations and Wider Applications

This study presents a detailed observational assessment of the Ekman drain for the Hebrides Shelf and indicates that there is a significant export of organic carbon to the open ocean, as well as significant variability in export fluxes along the shelf break. Nevertheless, the data set we present here is not perfect. Obvious weaknesses include the patchy VMADCP coverage, the horizontal sampling resolution, which was relatively crude compared to the width of the Slope Current, and the westward extent of sampling, which may not have fully resolved the true western boundary of the Slope Current on all transects. Nevertheless, our measurements of the Slope Current itself are comparable with previous observations and with recent modeled fluxes, and our carbon fluxes agree well with prior measurements and shelf-wide synthesis efforts, suggesting that the limitations of the data may not significantly impact the overall conclusions.

It is not appropriate however to extrapolate our observations more widely along the edge of the NW European shelf as both models and observations show that currents and transports tend to be weaker further south and significantly stronger further north. Consequently, we would overestimate fluxes in the south or underestimate them further north using the mean results obtained along the Hebrides Shelf. In addition, the 4-fold variability we report in the bottom Ekman transport and up to 9-fold variability in particulate concentrations argues for caution in regional or global extrapolations from limited data. However, poleward flowing Slope Currents are a common feature globally [Hill *et al.*, 1998] thus the potential magnitude of off-shelf carbon fluxes associated with the Ekman drain may be significant at a global level. Widely recognized limitations in data coverage though have to date prevented detailed quantification of the cross-shelf exchange of carbon at the global scale [Liu *et al.*, 2010 and references therein]. Nevertheless, a simple calculation using our mean Ekman drain transport estimate and carbon pool concentrations and a global shelf break length of 1.5×10^5 km [Jahnke, 2010] provides an order of magnitude estimate of total carbon flux of ~ 0.6 Pg C d^{-1} or ~ 230 Pg C yr^{-1} , the vast majority of which is DIC. This estimate, however, is 6.5 times larger than a global estimate of DIC transport reported by Chen *et al.* [2003] and neatly demonstrates how much we still have to learn about the coastal ocean.

5. Conclusions

During October and November 2014, the Hebrides Shelf was a moderate sink for atmospheric CO₂, with a mean shelf wide air-sea CO₂ flux of -3.2 mmol C $m^{-2} d^{-1}$. This equated to a total regional sink of -0.0021 Tg C d^{-1} , comparable to estimates derived from more extensive database analyses. Transport of carbon off shelf via the downwelling circulation that is typical of this shelf region, resulted in a total offshore carbon flux of 2.18 Tg C d^{-1} (4.21 tonnes C $m^{-1} d^{-1}$), of which 93.6% was inorganic and 6.4% was organic with DOC representing 95% of the organic flux. On a per unit area basis, the export of POC from the Hebrides Shelf of 10.01 mmol C $m^{-2} d^{-1}$ was found to be 5 times larger than the global mean. An equivalent calculation based on global shelf break length indicated the mean offshore POC flux of 12.75 kg C $m^{-1} d^{-1}$ was ~ 3 -fold larger than the global mean. Consequently, the total offshore POC flux of 0.007 Tg C d^{-1} could represent $\sim 1\%$ of total global downslope POC export making the Hebrides Shelf a potentially significant source of POC to the continental slope and neighboring northeast Atlantic Ocean. We estimate this mechanism could supply the ocean benthos with a daily average particulate carbon flux of 0.24 ± 0.18 g C $m^{-2} d^{-1}$.

References

- Artoli, Y., J. C. Blackford, G. Nondal, R. G. J. Bellerby, S. L. Wakelin, J. T. Holt, M. Butenschön, and J. I. Allen (2014), Heterogeneity of impacts of high CO₂ on the North Western European Shelf, *Biogeosciences*, *11*, 601–612.
- Barron, C., and C. M. Duarte (2015), Dissolved organic carbon pool and export from the coastal ocean, *Global Biogeochem. Cycles*, *29*, 1725–1738, doi:10.1002/2014GB005056.
- Bauer, J. E., W.-J. Cai, P. A. Raymond, T. S. Bianchi, C. S. Hopkinson, and P. A. G. Regnier (2013), The changing carbon cycle of the coastal ocean, *Nature*, *504*, 61–70.
- Baxter, J. M., I. L. Boyd, M. Cox, A. E. Donald, S. J. Malcol, H. Miles, B. Miller, and C. F. Moffat (2011), *Scotland's Marine Atlas: Information for the National Marine Plan*, 191 pp., Edinburgh, Marine Scotland.
- Booth, D. A., and D. J. Ellett (1983), The Scottish continental slope current, *Cont. Shelf Res.*, *2*(2/3), 127–146.
- Borges, A. V. (2005), Do we have enough pieces of the jigsaw to integrate CO₂ fluxes in the coastal ocean? *Estuaries*, *28*(1), 3–27.
- Carter, D. J. T., J. Loynes, and P. G. Challenor (1987), *Estimates of extreme current speeds over the continental slope off Scotland*, Rep. 239, 143 pp., Inst. of Oceanogr. Sci., Wormley, U. K.
- Chafik, L., T. Rossby, and C. Shrum (2014), On the spatial structure and temporal variability of poleward transport between Scotland and Greenland, *J. Geophys. Res. Oceans*, *119*, 824–841, doi:10.1002/2013JC009287.

Acknowledgments

We thank the following for access to data, ECMWF for the ERA-Interim product (<http://apps.ecmwf.int/datasets/>), the NOAA-ESRL Physical Sciences Division, Boulder, Colorado, for NCEP-II reanalysis products (<http://www.esrl.noaa.gov/psd/>), and global CO₂ records (<http://www.esrl.noaa.gov/gmd/ccgg/trends/global.html#global>). We also thank the anonymous reviewer, editor, and John Huthnance for comments on an earlier version of this paper. L.A. Salt held post-doctoral grants from the Conseil Général du Finister and Région Bretagne. Cruise DY017 was a NERC National Capability funded cruise conducted in support of the UK NERC/DEFRA cofunded Shelf Sea Biogeochemistry programme (NE/K001701/1). Data are available via the British Oceanographic Data Centre (www.bodc.ac.uk) or from the authors.

- Chen, C.-T. A., and S.-L. Wang (1999), Carbon, alkalinity and nutrient budgets on the East China Sea continental shelf. *J. Geophys. Res.*, *104*(C9), 20,675–20,686.
- Chen, C.-T. A., K.-K. Liu, and R. Macdonald (2003), Continental margin exchange, in *Ocean Biogeochemistry*, edited by M. J. R. Fasham, pp. 53–97, Springer, Berlin.
- Chen, C.-T. A., T.-H. Huang, Y.-C. Chen, Y. Bai, X. He, and Y. Kang (2013), Air-sea exchanges of CO₂ in the world's coastal seas, *Biogeosciences*, *10*, 6509–6544.
- Dickson, A. G., C. L. Sabine, and J. R. Christian (2007), Guide to best practices for ocean CO₂ measurements, *PICES Spec. Publ.* 3, 191 pp. [Available at http://cdiac.ornl.gov/oceans/Handbook_2007.html.]
- Dickson, R. R., W. J. Gould, C. Griffiths, K. J. Medler, and E. M. Gmitrowicz (1986), Seasonality in currents in the Rockall Channel, *Proc. R. Soc. Edinburgh*, *88B*, 103–125.
- Dickson, R. R., P. M. Kelly, J. M. Colebrook, W. S. Wooster, and D. H. Cushing (1988), North winds and production in the eastern North Atlantic, *J. Plankton Res.*, *10*(1), 151–169.
- Egbert, G. D., and S. Y. Erofeeva (2002), Efficient inverse modelling of barotropic ocean tides. *J. Atmos. Oceanic Technol.* *19*, 183–204.
- Egbert, G. D., A. Bennett, and M. Foreman (1994), TOPEX/Poseidon tides estimated using a global inverse model. *J. Geophys. Res.*, *99*, 24,821–24,852.
- Egbert, G. D., S. Y. Erofeeva, and R. D. Ray (2010), Assimilation of altimetry data for nonlinear shallow-water tides: Quarter-diurnal tides of the Northwest European Shelf. *Cont. Shelf Res.*, *30*, 668–679.
- Firing, E., and J. M. Hummon (2010), Shipboard ADCP measurements. The GO-Ship Repeat Hydrography Manual: A collection of expert reports and guidelines, *IOCCP Rep. 14, ICPO Publ. Ser. 134*, Version 1, 2010: 1–11. [Available at <http://www.go-ship.org/HydroMan.html>.]
- Green, D. R. H., M. J. Cooper, C. R. German, and P. A. Wilson (2003), Optimization of an inductively coupled plasma-optical emission spectrometry method for the rapid determination of high-precision Mg/Ca and Sr/Ca in foraminiferal calcite. *Geochem. Geophys. Geosyst.*, *4*(6), 8404, doi:10.1029/2002GC000488.
- Hill, A. E., B. M. Hickey, F. A. Shillington, P. T. Strub, K. H. Brink, E. D. Barton, and A. C. Thomas (1998), Eastern ocean boundaries, in *The Global Coastal Ocean: Regional Studies and Syntheses*, edited by A. R. Robinson and K. H. Brink, vol. 11, pp. 29–67, John Wiley, N. Y.
- Holliday, N. P., and S. A. Cunningham (2013), The Extended Ellett line: Discoveries from 65 years of marine observations west of the UK, *Oceanography*, *26*(2), 126–163.
- Holliday, N. P., S. A. Cunningham, C. Johnson, S. F. Gary, C. Griffiths, J. F. Read, and T. Sherwin (2015), Multi-decadal variability of potential temperature, salinity and transport in the eastern sub-polar North Atlantic. *J. Geophys. Res. Oceans*, *120*, 5945–5967, doi:10.1002/2015JC010762.
- Holligan, P. M. (1986), Phytoplankton distributions along the shelf break. *Proc. R. Soc. Edinburgh*, *88B*, 239–263.
- Holt, J., and R. Proctor (2008), The seasonal circulation and volume transport on the northwest European continental shelf: A fine-resolution model study, *J. Geophys. Res.*, *113*, C06021, doi:10.01029/02006JC004034.
- Holt, J., S. Wakelin, and J. Huthnance (2009), Down-welling circulation of the northwest European continental shelf: A driving mechanism for the continental shelf carbon pump, *Geophys. Res. Lett.*, *36*, L14602, doi:10.11029/12009GL038997.
- Huthnance, J. M. (1986), The Rockall slope current and shelf-edge processes, *Proc. R. Soc. Edinburgh*, *88B*, 83–101.
- Huthnance, J. M. (1995), Circulation, exchange and water masses at the ocean margin: The role of physical processes at the shelf edge, *Prog. Oceanogr.* *35*, 353–431.
- Huthnance, J. M. (2010), The northeast Atlantic margins, in *Carbon and Nutrient Fluxes in Continental Margins*, edited by K.-K. Liu et al., pp. 215–234, Springer, Berlin Heidelberg.
- Huthnance, J. M., and W. J. Gould (1989), On the northeast Atlantic Slope Current, in *Poleward Flows Along Eastern Ocean Boundaries*, edited by S. J. Neshyba et al., vol. 34, 374 pp., Coastal and Estuarine Stud.
- Huthnance, J. M., J. T. Holt, and S. L. Wakelin (2009), Deep ocean exchange with west-European shelf seas. *Ocean Sci.*, *5*, 621–634.
- Hydes, D. J., et al. (2010), Determination of dissolved nutrients (N, P, Si) in seawater with high precision and inter-comparability using gas-segmented continuous flow analysers. The GO-Ship Repeat Hydrography Manual: A collection of expert reports and guidelines, *IOCCP Rep. 14, ICPO Publ. Ser. 134*, Version 1, 2010: 1–87. [Available at <http://www.go-ship.org/HydroMan.html>.]
- Inall, M., P. Gillibrand, C. Griffiths, N. MacDougall, and K. Blackwell (2009), On the oceanographic variability of the North-West European Shelf to the west of Scotland. *J. Mar. Syst.*, *77*, 210–226.
- IOC SCOR and IAPSO (2010), The International Thermodynamic Equation of Seawater-2010: Calculation and use of thermodynamic properties, Intergovernmental Oceanographic Commission, 196 pp., *Manuals and Guides 56 UNESCO*.
- Jago, C. F., A. J. Bale, M. O. Green, M. J. Howarth, S. E. Jones, I. N. McCave, G. E. Millward, A. W. Morris, A. A. Rowden, and J. J. Williams (1993), Resuspension processes and seston dynamics, *Philos. Trans. R. Soc. A*, *343*, 475–491.
- Jahnke, R. A. (2010), Global synthesis, in *Carbon and Nutrient Fluxes in Continental Margins. Global Change: The IGBP Series*, edited by K.-K. Liu et al., pp. 597–615, Springer, Berlin.
- Jiang, L.-Q., W.-J. Cai, R. Wanninkhof, Y. Wang, and H. Luger (2008), Air-sea CO₂ fluxes on the U.S. South Atlantic bight: Spatial and seasonal variability, *J. Geophys. Res.*, *113*, C07019, doi:10.01029/02007JC004366.
- Kanamitsu, M., W. Ebisuzaki, J. Woollen, S.-K. Yang, J. J. Hnilo, M. Fiorino, and G. L. Potter (2002), NCEP-DOE AMIP-II Reanalysis (R-2), *Bull. Am. Meteorol. Soc.*, 1631–1643.
- Kirkwood, D. S. (1996), Nutrients: Practical notes on their determination in seawater. ICES Techniques in Marine Environmental Sciences Report 17. Copenhagen, International Council for the Exploration of the Seas, 25 pp.
- Langdon, C. (2010), Determination of dissolved oxygen in seawater by Winkler titration using the amperometric technique. The GO-Ship Repeat Hydrography Manual: A collection of expert reports and guidelines, *IOCCP Rep. 14, ICPO Publ. Ser. 134*, Version 1, 2010, pp. 1–18. [Available at <http://www.go-ship.org/HydroMan.html>.]
- Laruelle, G. G., R. Lauerwald, B. Pfeil, and P. Regnier (2014), Regionalized global budget of the CO₂ exchange at the air-water interface in continental shelf seas, *Global Biogeochem. Cycles*, *28*, 1199–1214, doi:10.1002/2014GB004832.
- Liu, K.-K., L. Atkinson, R. Quinones, and L. Talae-McManus (2010), *Carbon and Nutrient Fluxes in Continental Margins*, 741 pp., Springer, Berlin.
- McCubbin, D., K. S. Leonard, J. Brown, P. J. Kershaw, R. A. Bonfeld, and T. Peak (2002), Further studies of the distribution of technetium-99 and caesium-137 in UK and European coastal waters, *Cont. Shelf Res.*, *22*, 1417–1445.
- McKay, W. A., J. M. Baxter, D. J. Ellett, and D. T. Meldrum (1986), Radiocaesium and circulation patterns west of Scotland, *J. Environ. Radioact.*, *4*, 205–232.
- Orr, J. C., J.-M. Epitalon, and J.-P. Gattuso (2015), Comparison of ten packages that compute ocean carbonate chemistry, *Biogeosciences*, *12*, 1483–1510.

- Pelletier, G., E. Lewis, and D. Wallace (2007), *CO2SYS.XLS A Calculator for the CO₂ System in Seawater for Microsoft Excel/VBA*. Washington State Dep. of Ecol./ Brookhaven National Laboratory, Olympia, WA/Upton, N. Y.
- Pingree, R. D. (1993), Flow of surface waters to the west of the British Isles and in the Bay of Biscay, *Deep Sea Res., Part II*, 40(1–2), 369–388.
- Prandle, D. (1984), A modelling study of the mixing of ¹³⁷Cs in the seas of the European Continental Shelf, *Philos. Trans. R. Soc. A*, 310, 407–436.
- Proctor, R., F. Chen, and P. B. Tett (2003), Carbon and nitrogen fluxes across the Hebridean shelf break, estimated by a 2D coupled physical-microbiological model, *Sci. Total Environ.*, 314–316, 787–800.
- Ragueneau, O., and P. Treguer (1994), Determination of biogenic silica in coastal waters: Applicability and limits of the alkaline digestion method, *Mar. Chem.*, 45, 43–51.
- Raimbault, P., F. Diaz, W. Pouvesle, and B. Boudjellal (1999), Simultaneous determination of particulate organic carbon, nitrogen and phosphorus collected on filters, using a semi-automatic wet-oxidation method, *Mar. Ecol. Prog. Ser.*, 180, 289–295.
- Regnier, P., et al. (2013), Anthropogenic perturbation of the carbon fluxes from land to ocean, *Nat. Geosci.*, 6, 597–606.
- Simpson, J. H., and R. R. McCandliss (2013), “The Ekman Drain”: A conduit to the deep ocean for shelf material, *Ocean Dyn.*, 63, 1063–1072.
- Souza, A. J., J. H. Simpson, M. Harikrishnan, and J. Malarkey (2001), Flow structure and seasonality in the Hebridean slope current, *Oceanol. Acta* 24(Suppl.), S63–S76.
- Takahashi, T., et al. (2009), Climatological mean and decadal change in surface ocean pCO₂, and net sea-air CO₂ flux over the global oceans, *Deep Sea Res., Part II*, 56, 554–577.
- Thomas, H. E., Y. Bozec, K. Elkalay, and H. J. W. De Baar (2004), Enhanced open ocean storage of CO₂ from shelf sea pumping, *Science*, 304, 1005–1008.
- Thomas, H., Y. Bozec, H. J. W. de Baar, K. Elkalay, M. Frankignoulle, L.-S. Schiettecatte, G. Kattner, and A. V. Borges (2005), The carbon budget of the North Sea, *Biogeosciences*, 2, 87–96.
- Tsunogai, S., S. Watanabe, and T. Sato (1999), Is there a “continental shelf pump” for the absorption of atmospheric CO₂? *Tellus Ser. B*, 51, 701–712.
- Uchida, H., G. C. Johnson, and K. E. Mctaggart (2010), CTD oxygen sensor calibration procedures. The GO-Ship Repeat Hydrography Manual: A collection of expert reports and guidelines, *IOCCP Rep. 14, ICPO Publ. Ser. 134*, Version 1, 2010, pp. 1–17. [Available at <http://www.go-ship.org/HydroMan.html>.]
- Van Bleijswijk, J., R. Kempers, P. Van Der Wal, P. Westbroek, J. Egge, and T. Lukk (1994), Standing stocks of PIC, POC, PON and *Emiliania huxleyi* coccospheres and liths in seawater enclosures with different phosphate loadings, *Sarsia*, 79, 307–318.
- Wakelin, S. L., J. T. Holt, J. C. Blackford, J. I. Allen, M. Butenschon, and Y. Artioli (2012), Modeling the carbon fluxes of the northwest European continental shelf: Validation and budgets. *J. Geophys. Res.*, 117, C05020, doi:10.1029/2011JC007402.
- Wanninkhof, R. (1992), Relationship between wind speed and gas exchange over the ocean, *J. Geophys. Res.*, 97(C5), 7373–7382.
- Weiss, R. F. (1974), Carbon dioxide in water and seawater: The solubility of a non-ideal gas, *Mar. Chem.*, 2, 203–215.
- Weiss, R. F., and B. A. Price (1980), Nitrous oxide solubility in water and seawater, *Mar. Chem.*, 8, 347–359.
- White, M., and P. Bowyer (1997), The shelf-edge current north-west of Ireland, *Ann. Geophys.*, 15, 1076–1083.
- Xing, J., and A. M. Davies (1996), A numerical model of the long term flow along the Malin-Hebrides shelf, *J. Mar. Syst.*, 8, 191–218.
- Xu, W., P. I. Miller, G. D. Quartly, and R. D. Pingree (2015), Seasonality and interannual variability of the European Slope current from 20 years of altimeter data compared with in situ measurements, *Remote Sens. Environ.*, 162, 196–207.

Erratum

In the originally published version of this article, the unit measures of Figure 7 were published as of $\mu\text{mol L}^{-1}$. This has since been corrected, and this version may be considered the authoritative version of record.